AWARD NUMBER: W81XWH-17-1-0126

TITLE: Immune Checkpoint Regulator in Ovarian Cancer Progression

PRINCIPAL INVESTIGATOR: Samuel C. Mok

CONTRACTING ORGANIZATION: M.D. Anderson Cancer Center, University of Texas
Houston, TX 77030

REPORT DATE: May 2018

TYPE OF REPORT: Annual

PREPARED FOR: U.S. Army Medical Research and Materiel Command
Fort Detrick, Maryland 21702-5012

DISTRIBUTION STATEMENT: Approved for Public Release;
Distribution Unlimited

REPORT DOCUMENTATION PAGE

Form Approved
OMB No. 0704-0188

1. REPORT DATE	2. REPORT TYPE	3. DATES COVERED
May 2018	Annual	5/1/2017-4/30/2018

4. TITLE AND SUBTITLE
Immune Checkpoint Regulator in Ovarian Cancer Progression

5a. CONTRACT NUMBER

5b. GRANT NUMBER
W81XWH-17-1-0126

5c. PROGRAM ELEMENT NUMBER

6. AUTHOR(S)
Samuel C. Mok

E-Mail: scmok@mdandersob.org

5d. PROJECT NUMBER

5e. TASK NUMBER

5f. WORK UNIT NUMBER

7. PERFORMING ORGANIZATION NAME(S) AND ADDRESS(ES)
M.D. Anderson Cancer Center, University of Texas
1515 Holcombe Boulevard, Houston TX 77030

8. PERFORMING ORGANIZATION REPORT NUMBER

9. SPONSORING / MONITORING AGENCY NAME(S) AND ADDRESS(ES)

U.S. Army Medical Research and Materiel Command
Fort Detrick, Maryland, 21702-5012

10. SPONSOR/MONITOR'S ACRONYM(S)

11. SPONSOR/MONITOR'S REPORT NUMBER(S)

12. DISTRIBUTION / AVAILABILITY STATEMENT

Approved for Public Release; Distribution Unlimited

13. SUPPLEMENTARY NOTES

14. ABSTRACT
We hypothesize that CAF-derived MFAP5 can generate an immuno-suppressive microenvironment that suppresses $CD8^+$ CTL activation by up-regulating CD47 expression in ovarian tumor cells and $CD8^+$ CTLs and that inhibits $CD8^+$ CTL trafficking through the extracellular matrix in the ovarian tumor microenvironment. A majority of experiments proposed under Major Goal 1 and a subset of experiments proposed under Major Goal 3 has been accomplished. Our results demonstrated that a marked inverse correlation between stromal MFAP5 expression and intraepithelial $CD8^+$ T-cell density in high-grade serous ovarian tumor tissue samples. In addition, tumors developed in mice treated MFAP5-specific siRNAs or an anti-MFAP5 antibody had significantly lower CD47 expression levels than in those treated with the control siRNA or the control IgG antibody, respectively. Preliminary studies also demonstrated that markedly lower intratumoral $CD8^+$ T cell densities in mice treated with MFAP5-specific siRNAs than the control siRNA. Taken together, MFAP5 silencing or blockade in ovarian tumor bearing mice activate tumor infiltrating $CD8^+$ T cells and down-regulate CD47 expression in tumor tissue.

15. SUBJECT TERMS
Ovarian cancer, MFAP5, CD47, tumor microenvironment, CAF

16. SECURITY CLASSIFICATION OF:			17. LIMITATION OF ABSTRACT	18. NUMBER OF PAGES	19a. NAME OF RESPONSIBLE PERSON
a. REPORT	b. ABSTRACT	c. THIS PAGE			USAMRMC
Unclassified	Unclassified	Unclassified	Unclassified	47	19b. TELEPHONE NUMBER *(include area code)*

Table of Contents

Page

1. INTRODUCTION

Although a subset of patients with advanced high-grade serous ovarian cancer (HGSOC) survive more than 5 years, the vast majority have their cancers recur within 12-24 months after diagnosis and die of recurrent metastatic disease. The identification of predictive or prognostic markers for ovarian cancer is crucial for developing novel therapeutic targets and prolonging patient survival. Recent studies show that biomarkers expressed by specific stromal cell types in the tumor microenvironment may have prognostic value. The immune system is an important determinant of the tumor microenvironment; various immunologic gene products during ongoing inflammation create a favorable microenvironment for tumor growth and progression. Recent studies demonstrated that $CD8^+$ tumor-infiltrating lymphocytes are associated with improved overall survival and have been described in several solid tumors, including ovarian cancer. Nevertheless, the molecular mechanisms underlying the promotion or inhibition of $CD8^+$ lymphocyte infiltration in ovarian cancer are not fully understood. By analyzing the transcriptome profile of microdissected cancer-associated fibroblasts (CAFs) adjacent to tumor cells in ovarian tumor tissue from patients with HGSOCs, we identified a CAF gene signature associated with decreased intratumoral $CD8^+$ cytotoxic T cell (CTL) density. Among the genes in this signature, we found that high expression levels of CAF-derived microfibrillar-associated protein 5 (MFAP5), a 25-kD extracellular matrix glycoprotein with an RGD domain, has been shown to enhance the invasive potential of ovarian cancer cells through the $\alpha_v\beta_3$-dependent FAK/ERK/TNNC1 signaling pathway, were associated with decreased $CD8^+$ CTL density in the epithelial compartment of HGSOCs and with poor patient survival. Silencing MFAP5 in an ovarian cancer–bearing immuno-competent C57BL/6 mouse model significantly increased intraepithelial $CD8^+$ T cell density. Further functional studies showed that recombinant MFAP5 increased apoptosis in cultured $CD8^+$ T cells. Transcriptome profiling analysis showed a marked increase in the expression of CD47, a known immune checkpoint mediator that inhibits macrophage phagocytosis of tumor cells and deactivates $CD8^+$ T cells, in MFAP5-treated ovarian cancer cells and $CD8^+$ T cells. Correlative studies demonstrated significant correlations between higher CD47 expression in ovarian cancer cells, higher MFAP5 expression in CAFs, worse patient survival rates, and lower intraepithelial $CD8^+$ CTL density. We therefore hypothesize that CAF-derived MFAP5 can generate an immuno-suppressive microenvironment that suppresses $CD8^+$ CTL activation by up-regulating CD47 expression in ovarian tumor cells and $CD8^+$ CTLs and that inhibits $CD8^+$ CTL trafficking through the extracellular matrix in the ovarian tumor microenvironment. These effects, we hypothesize, lead to decreased intraepithelial $CD8^+$ CTL density and poor survival in patients with HGSOCs. MFAP5 blockade could therefore enhance $CD8^+$ CTL–mediated immune response and improve patient survival rates.

2. KEYWORDS

Ovarian cancer, MFAP5, CD47, tumor microenvironment, CAF

3. ACCOMPLISHMENTS

a. What were the major goals of the project?

Major Goal 1: Evaluate the effect of MFAP5 blockade on intraepithelial $CD8^+$ CTL density (Months 1-12).

Major Goal 2: Evaluate and compare the effect of MFAP5 blockade on ovarian tumor metastasis and survival and T cell deprived mice (Months 10-24).

Major Goal 3: Evaluate the effect of MFAP5 on CD47 expression and intraepithelial $CD8^+$ CTL density (Months 12-16).

Major Goal 4: Evaluate whether CD47 mediates the effect of MFAP5 in preventing macrophage phagocytosis of ovarian cancer cells and on $CD8^+$ CTL activation (Months 1-30).

Major Goal 5: Evaluate whether CD47 mediates the effect of MFAP5 in inducing apoptosis in $CD8^+$ CTLs (Months 20-30).

Major Goal 6: Evaluate the role of MFAP5 in inhibiting effector T cell trafficking through interstitial tissue space (Months 25-30).

Major Goal 7: Evaluate signaling pathways that mediate the effect of MFAP5 on CD47 expression in ovarian cancer cells and $CD8^+$ T cells (Months 24-30).

Major Goal 8: Evaluate the role of ovarian cancer cell-derived exosomes in up-regulating CD47 protein in $CD8^+$ T cells (Months 30-36).

b. What was accomplished under these goals?

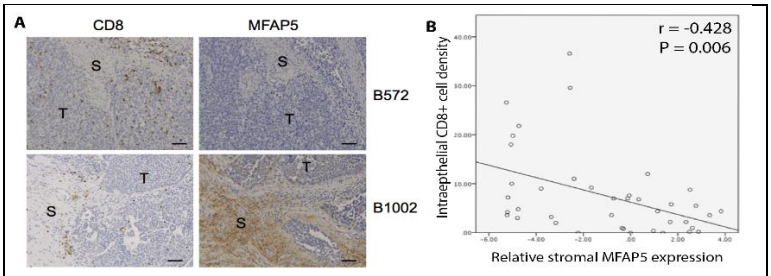

Fig. 1. A) Immunolocalization of $CD8^+$ CTLs and stromal MFAP5 in HGSOCs showing representative samples with high and low stromal MFAP5 (B572 and B1002, respectively) associated with low and high $CD8^+$ CTL densities, respectively. **B)** Correlation between stromal MFAP5 protein expression levels and intraepithelial $CD8^+$ CTL densities in 50 HGSOC patient samples. T: tumor, S: stroma

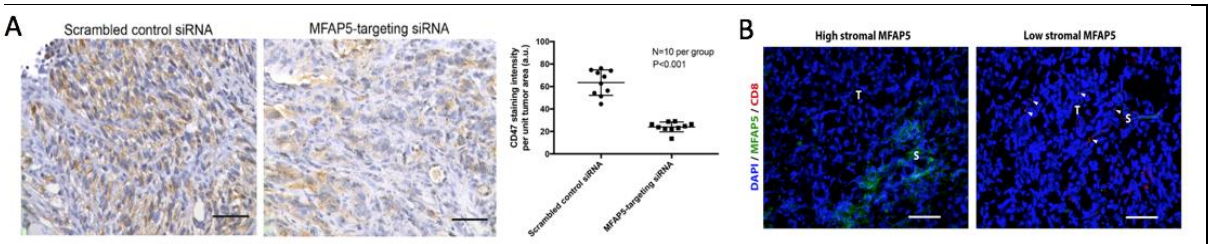

Fig. 2. A). Immunolocalization of CD47 expression in tumor tissue obtained from mice treated with MFAP5 specific siRNAs or a control siRNA. **B).** Immunofluorescent labeling of

$CD8^+$ T cells showing markedly increased in number of $CD8^+$ T cells in the tumor tissues obtained from mice treated with MFAP5 specific siRNAs compared with those treated with the control siRNA.

A majority of experiments proposed under Major Goal 1 and a subset of experiments proposed under Major Goal 3 has been accomplished. To identify CAF-specific genes associated with differential immune responses in ovarian tumors, correlative studies of genes in the CAF transcriptome signature and of the number of intraepithelial $CD8^+$ T cells in HGSOCs were performed by our group. The results demonstrated a marked inverse correlation between stromal MFAP5 expression and intraepithelial $CD8^+$ T-cell density in HGSOCs. These results were confirmed by the correlation of stromal MFAP5 protein expression and intraepithelial $CD8^+$ T cell density (**Fig. 1**). To validate the association between MFAP5 expression and $CD8^+$ T cell density, MFAP5 was silenced in ovarian cancer-bearing mice to determine its effect on the number of $CD8^+$ T cells in ovarian tumors. Immuno-competent Dicer/Pten/$P53^{(R172H)}$ triple-mutant C57BL/6 mice with ovarian tumors were injected intravenously with MFAP5-specific small interference RNAs (siRNAs) or control siRNAs encapsulated in chitosan nanoparticles (NPs). CD47 protein expression in tumor cells and $CD8^+$ T cell densities were determined. The results showed that tumors developed in mice treated MFAP5 specific siRNAs (N = 10) had significantly lower CD47 expression levels than in those treated with the control siRNA (P<0.001) (**Fig. 2A**). Quantification of intratumoral CD8+ T cells is ongoing. Preliminary data analyses on $CD8^+$ T cell densities showed markedly increased in number of $CD8^+$ T cells in the tumor tissues obtained from mice treated with MFAP5 specific siRNAs compared with those treated with the control siRNA (**Fig. 2B**).

In addition to determine the effect of MFAP5 silencing using MFAP5-specific siRNAs on CD47 expression in tumor cells, anti-MFAP5 antibodies was also used to determine the effect of circulating MFAP5 blockade on CD47 expression and $CD8^+$ T cell densities in tumor tissues developed from mice. The results showed a significant lower in CD47 expression in tumor tissue obtained from mice treated with an anti-MFAP5 antibody than in those treated with the control IgG (P<0.001) (**Fig. 3**). Quantification on $CD8^+$ T cells in tumor tissue is on-going.

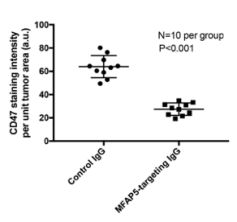

Fig. 3. Box plot showing significant lower CD47 protein expression in in tumor tissue obtained from mice treated with an anti-MFAP5 antibody than in those treated with the control IgG (P<0.001).

c. What opportunities for training and professional development has the project provided?

Nothing to report

d. How were the results disseminated to communities of interest?

Nothing to report

e. What do you plan to do during the next reporting period to accomplish the goals?

During the next reporting period (months 12-24), we will perform experiments according to those outlines in the proposal to further delineate the role of MFAP5 and CD47 in suppressing T cell activation and trafficking in ovarian tumor tissue.

4. IMPACT

a. What was the impact on the development of the principal disciplines of the project?
Nothing to report

b. What was the impact on other disciplines?
Nothing to report

c. What was the impact on technology transfer?
Nothing to report

d. What was the impact on society beyond science and technology?
Nothing to report

5. CHANGES/PROBLEMS

Nothing to report

6. PRODUCTS

a. Publications

Leung CS, Yeung TL, Yip KP, Wong, KK, Ho SY, Mangala LS, Sood AK, Lopez-Berestein G, Sheng J, Wong ST, Birrer MJ, Mok SC. Cancer-associated fibroblasts regulate endothelial adhesion protein LPP to promote ovarian cancer chemoresistance. J Clin Invest. 2018;128(2):589-606. PubMed PMID: 29251630; PubMed Central PMCID:PMC5785271.

7. PARTICIPANTS & OTHER COLLABORATING ORGANIZATIONS

a. What individuals have worked on the project?

Samuel C. Mok: no change
Shao-Cong Sun: no change
Tsz-Lun Yeung: no change
Stephen Wong: no change

b. Has there been a change in the active other support of the PD/PI(s) or senior/key personnel since the last reporting period?

The updated other support documents were attached.

c. What other organizations were involved as partners?

Nothing to report

Samuel C. Mok, Ph.D.

Past Support (past 5 years)

Title: Project 3 Personalized Therapies for Low-Grade Ovarian Serous Carcinomas
Funding agency: P50CA083639-15, The University of Texas MD Anderson Ovarian Cancer SPORE
Award dates: 2010/09/01-2015/08/31
Program officer: Kuzmin, Igor, A. Kuzmini@mail.nih.gov
PI: Bast, Robert
Goal: The major goal of this project is to develop new strategies in the treatment of low-grade serous ovarian cancer.
Specific aims:
Aim 1: To identify genomic and proteomic predictors of anti-tumor efficacy of the MEK inhibitor AZD6244 using GOG 0239 specimens.
Aim 2: To investigate the functional role of FOXO3a in conferring resistance to inhibitors of PISK/AKT and MEK/ERK kinases in low-grade ovarian cancer cells.
Aim 3: To investigate the IGF1-P13K pathway as a potential therapeutic target for low-grade OSC.
Aim 4: To develop clinical trials involving novel combined targeted agent approaches.
Effort: 0.84 CM
Direct cost: $189,000
Role: Co-PL

Title: Prognostic markers for ovarian cancer
Funding agency: R01 CA 133057-01A1, NIH/NCI
Award dates: 2009/03/01-2014/12/31
Program officer: Kelly, Kim Y., kimke@mail.nih.gov
PI: Mok, Samuel
Goal: The goal of this study is to functionally characterize prognostic markers identified in high-grade serous ovarian cancer using mouse models.
Specific aims:
Aim 1: Verify the correlation between DNA copy number abnormalities and expression levels of genes located in the 12 CGH segments that are associated with overall survival in patients with high-grade advanced stage serous adenocarcinomas.
Aim 2: Perform further validation studies utilizing an independent set of samples obtained from patients entered on Gynecologic Oncology Group (GOG) protocol 218 and to develop a genetic based prognostic model for high-grade advanced stage serous adenocarcinomas.
Aim 3: Validate the prognostic value of each candidate marker using genetically characterized ovarian cancer cell lines and orthotopic mouse models.
Effort: 1.2 CM
Direct cost: $181,148
Role: PI

Title: UCHL-1 As a Potential Therapeutic Target in Uterine Papillary Serous Carcinoma, Uterine SPORE Development

Funding agency: P50CA098258, NIH/NCI
Award dates: 2013/09/01-2014/08/31
Program officer: N/A
PI: Lu, Karen
Goal: The major goal is to evaluate whether targeting UCHL-1 can be used in the treatment of uterine papillary serous carcinoma.
Specific aims:
Aim 1: To further delineate the functional role of UCHL1 in UPSC cell proliferation and invasion potential using both *in vitro* and orthotopic mouse models.
Aim 2: To delineate the underlying molecular mechanisms by which UCHL1 promotes UPSC cell growth and invasion.
Aim 3: To use both *in vitro* and *in vivo* models to evaluate the efficacies of UCHL1 inhibition alone or in combine with mTOR inhibitors in UPSC treatment.
Effort: 0.12 CM
Direct cost: $46,284
Role: PI

Title: Genomic stratification of ovarian cancer patients
Funding Agency: RC4CA156551, NIH/NC
Award dates: 2010/12/01-2013/11/30
Agency Contact and Address: NA
Goals and Aims: The major goal of this project is to validate gene signatures that can be used to stratify high-grade serous ovarian cancer patients for their treatment.
Aim 1: To validate the prognostic gene signature using clinical trial specimens obtained from patients entered into the Gynecologic Oncology Group (GOG) protocol 218.
Aim 2: To validate genes whose expression predicts for resistance to chemotherapy using Gynecologic Oncology Group (GOG) protocol 218.
Time Commitment: 2.4 CM
Direct cost: $154,529
Role: Co-I

Current Support

Title: Study of Biomarkers in Ovarian Cancer: Modulation by Activity and Diet Intervention
Funding agency: R01CA184918, NIH/NCI
Award dates: 2014/09/01-2020/08/31
Program officer: Ross, Sharon A. sr75k@nih.gov
PI: Thomson, Cynthia
Goal: The major goal is to evaluate the effect of diet and exercise on ovarian cancer progression.
Specific Aims:
Aim 1:To determine if the LIVES intervention alters biomarkers of metabolic deregulation in women previously treated for stage II-IV ovarian cancer
Aim 2: To determine if any effect of the intervention on biomarkers is mediated by change in central adiposity

Aim 3: To determine if any effect of the intervention on biomarkers is modified by baseline central adiposity including exploration of central adiposity using Computerized Tomography (CT) scans.
Effort: 0.24 CM
Direct cost: $3,238,945
Role: Co-I

Title: The FGF18/FGFR4 Amplicon: Novel Therapeutic Biomarkers for Ovarian Cancer
Funding agency: R01 CA169200-02, NIH/ NCI
Award dates: 2013/03/01-2019/02/28
Program officer: Kim, Kelly, Y. kimke@mail.nih.gov
PI: Mok, Samuel, Birrer, Michael
Goal: The major goal is to evaluate the functional role of FGF18 in ovarian cancer progression.
Specific aims:
Aim 1: To validate the prognostic value of FGF18/FGFR4 axis using a large collection of multi-center clinical trial specimens (GOG218)
Aim 2: To delineate the functional role and signaling network of FGF18 in ovarian tumor cells and ovarian tumor stromal cells in vitro and in vivo
Aim 3: To use the recently developed FGF trap proteins (from Five Prime Therapeutics Inc.) as proof of principle to target FGF18 as a novel therapeutic intervention against epithelial ovarian cancer.
Effort: 2.4 CM
Direct cost: $1,411,165
Role: Co-PI

Title: The Genomic, Epigenomic and Psychosocial Characteristics of Long-Term Survivors of Ovarian Cancer.
Funding agency: W81XWH-16-2-0038, DOD
Award dates: 2016/09/30-2020/09/29
Program Officer: NA
PI: Birrer, Michael
Goal: The overall goal of this multi-institutional proposal is to enhance the understanding of the molecular, biologic and patient-reported outcome characteristics of long-term survivors of ovarian cancer.
Specific aims:
Aim 1: To study the genomic characteristics (in terms of micro RNA expression) of long-term versus short-term survivors of ovarian cancer.
Aim 2: Investigate the research data generated by other members of the consortium, predictive biomarkers for long-term ovarian cancer survival will be identified for better stratification and prognostication and more effective treatment of ovarian cancer patients.
Effort: 0.6 CM
Direct cost: $62,500
Role: Co-I

Title: P1-The University of Texas MD Anderson Cancer Center SPORE in Uterine Cancer: Targeted Strategies for Prevention and Therapeutics for Hyperplasia and Grade 1 Endometrioid Endometrial Cancer.
Funding agency: P50CA098258, NIH/NCI
Award dates: 2016/09/01-2021/08/31
Program officer: Kuzmin, Igor, A. Kuzmini@mail.nih.gov
PI: Lu, Karen
Goal: The major role of this project is to develop new strategies in the treatment of grade 1 endometrial cancer.
Specific aims:
Aim 1: To conduct a clinical trial to evaluate an mTOR inhibitor (everolimus) in addition to levonorgestrel IUD for prevention/treatment of progestin-resistant CAH/grade 1 EEC
Aim 2: To evaluate the molecular basis underlying response to chemoprevention for CAH and reversal of Grade 1 EEC
Aim 3: To develop a novel intrauterine drug delivery approach for targeted chemoprevention and therapeutics for CAH and Grade 1 EEC
Effort: 2.4 CM
Direct cost: $300,000
Role: Co-I

Title: Immune Checkpoint Regulator in Ovarian Cancer Progression
Funding Agency: W81XWH-17-1-0126, DOD
Award dates: 2017/05/01-2020/04/30
Program officer: Dellinger, Susan M, susan.dellinger@us.army.mil
PI: Mok, Samuel
Goal: The overall goal of this proposal is to determine the molecular mechanism by which MFAP5 suppresses CD8+ T cell activation and trafficking in ovarian tumor tissue
Specific aims:
Aim 1: Determine the role of stromal MFAP5 in modulating CD8+ CTL activation in ovarian tumors *in vitro* and *in vivo.*
Aim 2: Identify the molecular mechanism by which MFAP5 modulates CD8+ CTL activation and trafficking in ovarian tumors *in vitro* and *in vivo.*
Aim 3: Determine the molecular mechanism by which MFAP5 upregulates CD47 in ovarian cancer cells and CD8+ CTLs.
Effort: 1.2 CM
Direct cost: $78,225
Role: PI

Title: The Role of Mesothelial Omentin in Ovarian Cancer Progression
Funding Agency: W81XWH-17-1-0146, DOD
Award dates: 2017/05/01-2020-04/30
Program officer: Dellinger, Susan M
PI: Yip, Daniel, Mok, Samuel
Goal: The overall goal of this proposal is to delineate the molecular mechanism by which omentin suppresses ovarian cancer progression

Specific aims:
Aim 1: Evaluate the mechanisms of action by which ITLN1 suppresses ovarian cancer cell motility and invasive potential.
Aim 2: Evaluate the mechanisms by which ITLN1 regulates ovarian cancer cell growth.
Aim 3: Evaluate the tumor suppressor role of ITLN1 in vivo and the efficacy of using ITLN1 in the treatment of ovarian cancer.
Effort: 1.2 CM
Direct cost: $45,000
Role: Co-PI

Title: P3-Overcoming MEK inhibitor resistance in low-grade ovarian serous carcinomas.
Funding Agency: 2P50CA083639-16A1, NIH/NCI
Award dates: 2017/09/01-2022/08/31
Agency Contact and Address: Kuzmin, Igor, A. Kuzmini@mail.nih.gov
PI: Bast, Robert
Goals and Aims: To understand the molecular responses of the tumor to trametinib treatment, we will obtain a post-progression biopsy from patients treated at MD Anderson while still on treatment under GOG 281.
Aim 1: To identify pathways altered in MEKi-treated cells using genomic, proteomic and biochemical approaches.
Aim 2: To investigate whether alternative pathways identified in aim 1 are associated with MEKi resistance using patient samples from GOG 281, patient samples from a proposed companion trail, and MEKi-resistant low-grade OSC cell lines that we have developed.
Aim3: To develop novel trials of MEKi combined with another drug to overcome MEKi resistance and the identification of MEKi independent pathway as novel targets.
Effort: 0.84 CM
Direct cost: $230,152
Role: Co-PI

Pending

Title: TuMIR Project 2: Cancer Associated Fibroblast and Immunosuppressive Tumor Microenvironment
Funding Agency: NIH/NCI
Award dates: 2017/12/01-2022/11/30
Program Officer: Dan Gallahan, Dan.Gallahan@nih.gov
PI: Nagrath D (Rice)
Goal: To determine the activation of cancer/stromal cell crosstalk signaling networks generates an immunosuppressive microenvironment in different compartments of ovarian tumors.
Specific aims:
Specific Aim 2: Uncover differential crosstalk signaling networks among various cell types within HGSOCs associated with decreased intraepithelial CD8+ T cell density and evaluate the CAF specific gene perturbation effect on the networks and CD8+ T cell activation and trafficking.

Specific Aim 3: Identify and evaluate the efficacy of repositioned drugs targeting activated crosstalk signaling networks linking CAFs and other stromal and cancer cells that are associated with low intraepithelial CD8+ T cell density.
Effort: 4.8 CM
Direct cost: $300,000
Role: Co-PI

Title: Predicting and targeting exosome-mediated crosstalk in ovarian cancer microenvironment
Funding Agency: U01CA232151, NCI/NIH
Award dates: 7/1/2018-6/30/2023
Program Officer: Shannon Hughes, 240-276-6224
PI: Wong, Stephen / Mok, Samuel
Goals and aims:
1. Develop computational modeling methods to identify exosome-mediated crosstalk between HGSC cells and CAF or CAA, and determine the role of CAF- and CAA-derived exosomes on tumor progression and chemoresistance.
2. Identify the receptor-based signaling pathways in HGSC cells modulated by CAF- and CAA-derived exosomal ncRNA-mediated pathways.
3. Identify therapeutic agents that target stromal-derived ncRNAs and major signaling pathways, and evaluate their effects in tumor progression and chemoresistance in HGSC animal models.
Effort: 3.0 CM
Direct cost: $240,000
Role: MPI

Overlap

None

PREVIOUS/CURRENT/PENDING

SUN, SHAO-CONG

PREVIOUS

RP150235 (Sun) 3/1/2015-2/28/2018 1.80 calendar
Cancer Prevention & Research Institute of Texas (CPRIT) $284,811
Role of TBK1 in Regulating and Dendritic Cell Function and Antitumor Immunity
Major goal(s): Study the signaling mechanism that regulates the function of dendritic cells (DCs) in the activation of antitumor T-cell responses.
Role: Principal Investigator
Specific Aim(s): 1) Understand how TBK1 negatively regulates costimulatory molecules and how TBK1 mediates induction of IDO by PRRs; to systematically define the TBK1-regulated genes in DCs by RNA sequencing, 2) Determine the DC-specific function of TBK1 in regulating the T-cell activation and effector T cell generation using *in vivo* and *in vitro* models and to generate animal models of tumor immunotherapy; and 3) Examine whether genetic ablation and pharmacological inhibition of TBK1 promotes rejection of preformed tumors by employing vaccine- and DC-based animal models of tumor immunotherapy.
Program Official Information: Name: Willson, James K.V., Chief Scientific Officer; Phone: (512) 305-8490

4R01GM084459-14 (Sun) 12/7/2012-11/30/2017 1.20 calendar
NIH/NIGMS $200,000
Molecular Mechanisms Regulating Noncanonical NF-kB Signaling
Major goal(s): Characterize the molecular mechanisms mediating the negative regulation of signal-induced noncanonical NF-kB activation.
Role: Principal Investigator
Specific Aim(s): 1) Elucidate the biochemical mechanisms that regulate the signaling function of NIK, 2) Characterize the intermediate signaling steps and molecular components of the noncanonical NF-kB pathway; and 3) Investigate the role of noncanonical NF-kB pathway in normal and pathological T-cell activation.
Program Official Information: Name: Melillo, Amanda A.; Phone: 301-594-9718; Email: amanda.melillo@nih.gov

RP140244 (Sun) 8/31/2014-8/30/2017 1.80 calendar
Cancer Prevention & Research Institute of Texas (CPRIT) $275,513
Regulation of MDM2-Mediated Oncogenesis and Anti-Tumor Immunity by USP15
Major goal(s): 1) Investigate how USP15 exerts these intriguing functions and to evaluate USP15 as a therapeutic target using clinically relevant animal models of cancer therapy; and 2) Screen for small-molecule inhibitors of USP15 and examine their therapeutic potential.
Role: Principal Investigator
Specific Aim(s): 1) Define the mechanism by which USP15 regulates MDM2 stability and cancer cell survival, 2) Examine how USP15 regulates T-cell activation and anti-tumor immunity; and 3) Evaluate USP15 as a therapeutic target in cancer treatment using clinically relevant animal models of cancer immunotherapy and to obtain and apply small-molecule inhibitors of USP15 or therapeutic siRNAs to the therapeutic studies.
Program Official Information: 1701 North Congress Avenue, Suite 6-127, Austin, TX 78701; Phone: 512-463-3190; Email: cprit@cprit.state.tx.us

5R01AI090113-05 (Cheng) 9/15/2010-8/31/2015 0.60 calendar
NIH/NIAID $349,719
Linking IKKbeta Activation to Anti-Autophagy in Viral Protein Tax-Mediated Oncoge
Major goal(s): Decipher the pathological role of the axis of Tax- IKK(-BECN1/Bif-1 in HTLV-1 oncogenesis.
Role: Subrecipient Principal Investigator
Specific Aim(s): 1) Define the domain critical for lipid raft targeting of Tax1, 2) Investigate the underlying mechanism of Tax1 to deregulate autophagy; and 3) Determine oncogenic potential and anti-autophagy function of lipid raft-targeted IKK(.
Program Official Information: Park, Eun-Chung; Phone: 301-496-7453; Email: epark@niaid.nih.gov

5R01AI064639-09 (Sun) 7/1/2010-6/30/2015 2.75 calendar

NIH/NIAID $253,703
Regulation of T-cell Function and Autoimmune Inflammation by Deubiquitinase CYLD
Major goal(s): Understand the molecular mechanism by which CYLD regulates T-cell development and activation.
Role: Principal Investigator
Specific Aim(s): 1) Examine the molecular mechanism and functional significance of CYLD-mediated NF-κB regulation in T cells, 2) Characterize the molecular and cellular mechanisms by which CYLD regulate T-cell tolerance and inflammatory T-cell differentiation; and 3) Examine the immunological and osteoclast-intrinsic mechanisms by which CYLD regulates bone erosion.
Program Official Information: Lapham, Cheryl K., Phone: 240-627-3490; Email: clapham@mail.nih.gov

5R01AI057555-11 (Sun) 12/1/2009-11/30/2014 2.40 calendar
NIH/NIAID $250,000
The IKK/Tp12 Axis of TLR Signaling
Major goal(s): Elucidate the mechanism by which IκB kinase (IKK) and Tpl2 signaling axis regulates toll-like receptor (TLR) signaling in macrophages.
Role: Principal Investigator
Specific Aim(s): 1) Examine the molecular mechanism of IKK-dependent Tpl2 activation, 2) Examine the role of IKK in regulating the fate of Tpl2; and 3) Examine how the IKK/Tpl2 signaling axis is regulated by upstream TLR signals.
Program Official Information: Name: Palker, Thomas J.; Phone: 240-627-3542; Email: palkert@niaid.nih.gov

(Sun) 10/1/2012-9/30/2014 2.75 calendar
MD Anderson Cancer Center $100,000
Oncogenic Activation of Noncanonical NF-kB in B-cell Lymphomas
Major goal(s): Understand the role the noncanonical NF-kB pathway in B-cell lymphoma regulation.
Role: Principal Investigator
Specific Aim(s): 1) Examine the role of noncanonical NF-κB pathway in B-cell lymphomagenesis using mouse models and human lymphoma cells; and 2) Characterize novel regulators of the noncanonical NF-κB signaling and examine their association with human B-cell lymphomas.
Program Official Information: 1515 Holcombe Boulevard, Houston, TX 77030; Phone: 713-792-2121

(Sun) 9/1/2011-8/31/2013 2.75 calendar
G.S. Hogan Gastrointestinal Research Fund, MD Anderson Cancer Center $100,000
Regulation of Colon Inflammation and Tumorigenesis by Tumor Suppressor CYLD
Major goal(s): Elucidate the cellular and molecular mechanisms by which CYLD regulates colon tumorigenesis.
Role: Principal Investigator
Specific Aim(s): 1) Create conditional CYLD knockout (KO) mice to specifically ablate CYLD in immune cells, IECs, and ISCs; and 2) Examine the signaling mechanisms of CYLD function.
Program Official Information: 1515 Holcombe Boulevard, Houston, TX 77030; Phone: 713-792-2121

(Sun) 7/1/2008-10/31/2012 2.40 calendar
NIH/NIGMS $800,000
Molecular Mechanisms Mediating NF-kB/p100 Processing
Major goal(s): Understand the molecular mechanism regulating p100 processing.
Role: Principal Investigator
Specific Aim(s): 1) Define the negative- and positive-regulatory sequences of p100 processing, 2) Identify and characterize cellular factors regulating the processing of p100; and 3) Investigate how the GRR regulates p100 processing.
Program Official Information: 45 Center Drive MSC 6200, Bethesda, MD 20892-6200

(Sun) 9/30/2009-8/31/2011 0.45 calendar
NIH/NIGMS $400,000
Signaling Mechanism by which NIK Regulates EAE
Major goal(s): Understand how the kinase NIK regulates the pathogenesis of EAE, an animal model of multiple sclerosis.

Role: Principal Investigator
Specific Aim(s): 1) Determine the mechanism and functional significance of NIK-mediated STAT3 activation in CD4 T cells, 2) Examine the role of noncanonical NF-κB in the regulation of Th17 differentiation and EAE pathogenesis, 3) Examine the role of TRAF3 in NIK regulation and Th17 cell differentiation; and 4) Define the domains/motifs of NIK that are required for its Th17-regulatory function.
Program Official Information: 45 Center Drive MSC 6200, Bethesda, MD 20892-6200

(Sun) 3/1/2009-2/28/2011 0.45 calendar
Amgen $50,000
Mechanism of CYLD-Mediated Apoptosis and Tumor Suppression
Major goal(s): Understand the molecular mechanism by which CYLD promotes apoptosis and inhibits tumorigenesis.
Role: Principal Investigator
Specific Aim(s): 1) Elucidate the molecular mechanism and functional significance of CYLD/RIP1 interplay, 2) Examine the mechanism and functional significance of TBK1/IKKe aberrant activation in CYLD-deficient cells; and 3) Examine the tumor suppressor role of CYLD using mouse models.
Program Official Information: One Amgen Center Drive, Thousand Oaks, CA 91320-1799

CURRENT

2R01GM084459-15 (Sun) 10/2/2017-10/1/2022 1.80 calendar
NIH/NIGMS $250,000
Molecular Studies of Noncanonical NF-kb Signaling
Major goal(s): Characterize novel regulators and functions of the noncanonical NF-kB pathway.
Role: Principal Investigator
Specific Aim(s): 1) Elucidate the mechanism by which noncanonical NF-κB functions in DCs to regulate mucosal immunity, 2) Characterize novel factors that regulate noncanonical NF-κB signaling; and 3) Investigate the immunoregulatory functions of novel noncanonical NF-κB regulators.
Program Official Information: Name: Somers, Scott D.; Phone: (301) 594-3827; Email: somerss@nigms.nih.gov

5R37AI064639-12 (Sun) 7/1/2015-6/30/2020 1.36 calendar
NIH/NIAID $250,000
Regulation of T-Cell Function and Autoimmune Inflammation by Deubiquitinases
Major goal(s): Understand the molecular mechanisms by which Otud7b and Usp4/Usp15 regulate T-cell receptor (TCR) signaling and T cell-mediated immunity and autoimmune inflammation.
Role: Principal Investigator
Specific Aim(s): 1) Define the molecular mechanism by which Otud7b mediates TCR signaling, 2) Examine how Usp4 and USP15 negatively regulate TCR signaling; and 3) Investigate *in vivo* functions of Otud7b and Usp4 in regulating T-cell function and autoimmune inflammation.
Program Official Information: Name: Ramachandra, Lakshmi; Phone: 240-669-5061; Email: Ramachandral@niaid.nih.gov

W81XWH-17-1-0126 (Mok) 5/1/2017-4/30/2020 0.36 calendar
US Department of Defense (DoD) $150,000
OC160042: Immune Checkpoint Regulator in Ovarian Cancer Progression
Major goal(s): Determine the role and molecular mechanisms of stromal MFAP5 in modulating CD8+ CTL activation in ovarian tumors *in vitro* and *in vivo*.
Role: Co-Investigator
Specific Aim(s): 1) Determine the role of stromal MFAP5 in modulation of CD8+ CTL activation in ovarian tumors, 2) Identify the molecular mechanism by which MFAP5 modulates CD8+ CTL activation and trafficking in ovarian tumors *in vitro* and *in vivo*; and 3) Determine the molecular mechanism by which MFAP5 up-regulates CD47 in ovarian cancer cells and CD8+ CTLs.
Program Official Information: Name: Dellinger, Susan M.; Phone: 301-619-2090; Email: susan.dellinger@us.army.mil

5R01AI057555-15 (Sun) 2/1/2015-1/31/2020 1.80 calendar

NIH/NIAID $250,000
Molecular Mechanisms Regulating TLR Signaling and Macrophage Activation
Major goal(s): Understand how TRAF2 and the deubiquitinase Zranb1 regulate TLR signaling and macrophage activation.
Role: Principal Investigator
Specific Aim(s): 1) Elucidate the mechanism by which TRAF2 regulates TLR signaling in macrophages, 2) Define the molecular mechanism by which Zranb1 mediates TLR signaling; and 3) Investigate the *in vivo* pathophysiological functions of TRAF2 and Zranb1 in myeloid cells.
Program Official Information: Name: Jiang, Chao; Phone: 301-761-7802; Email: jiangc3@mail.nih.gov

54217 (Sun) 9/27/2017-9/26/2019 0.24 calendar
Mission Therapeutics, Inc. $132,706
Characterization of DUB Inhibitors in Inflammation and Tumorigenesis
Major goal(s): Characterize Cezanne inhibitors in the regulation of T cell activation and differentiation, as well as cancer cell growth/survival using *in vitro* approaches.
Role: Principal Investigator
Specific Aim(s): 1) T cell activation and differentiation; and 2) Cancer studies.
Program Official Information: Name: CEO, Mission Therapeutics; Phone: +44 (0) 01223 607340

5P30CA016672-42 (Pisters) 9/1/2016-8/31/2019 0.60 calendar
NIH/NCI $200,000
Cancer Center Support Grant (CCSG) – Yee MRP - Immunotherapy of Pancreatic Cancer
Major goal(s): Develop effective immune-based therapies for pancreatic cancer involving modulation of both stimulatory and inhibitory immune checkpoints, augmentation of antigen-specific cellular responses, and innovative approaches to primary and secondary cancer immunoprevention.
Role: Co-Investigator
Specific Aim(s): 1) Test the preclinical efficacy of oral RORgt small molecule inhibitors for primary immunoprevention, 2) Define the checkpoint molecules landscape in the multistep progression from PanINs to PDAC for rational design of targeted approaches to primary immunoprevention; and 3) Characterize immune infiltrates and checkpoint molecules expression in liver micro-metastasis for the design of approaches to secondary immunoprevention.
Program Official Information: Name: Shafik, Hasnaa; Phone: 240-276-5600; Email: shafikh@mail.nih.gov

LS2017-00053496-AM1-JW (Sun) 6/26/2017-6/25/2018 0.12 calendar
Bridge Biotherapeutics, Inc. $156,250
Treatment of Immunological Disorders by BBT-401
Major goal(s): Investigate how BBT-401 modulates immune responses in inflammatory diseases, focusing on an animal model of multiple sclerosis (MS), experimental autoimmune encephalomyelitis (EAE).
Role: Principal Investigator
Specific Aim(s): 1) Examine how BBT-401 regulates innate immune response and CNS inflammation *in vivo*; and 2) Examine whether BBT-401 regulates microglia-mediated CNS inflammation.
Program Official Information: Name: Mikyoung Chang; Address: 2450 Holcombe Blvd, Suite J, Houston, TX 77021; Email: VP Research@Bridge Biotherapeutics

5R01AI104519-05 (Sun) 5/15/2013-4/30/2018 1.80 calendar
NIH/NIAID $263,146
Signaling Functions of Peli Family of E3 Ubiquitin Ligases
Major goal(s): Understand how Peli1 exerts its immunoregulatory functions.
Role: Principal Investigator
Specific Aim(s): 1) Examine how Peli1 regulates T-cell activation and tolerance, 2) Examine how Peli1 regulates innate immune receptor signaling and CNS inflammation; and 3) Elucidate the biochemical mechanisms regulating the activation and function of Peli1.
Program Official Information: Name: Esch, Thomas R.; Phone: 240 627 3565; Email: tesch@niaid.nih.gov

PENDING
(Mok) 4/1/2019-3/31/2024 0.60 calendar

University of Alabama Birmingham $160,000
Novel Immune Checkpoint Biomarkers in Ovarian Cancer
Major goal(s): Investigate and evaluate an immune checkpoint biomarker MFAP5 in ovarian cancer.
Role: Co-Investigator
Specific Aim(s): 1) Delineate the molecular mechanism by which MFAP5 confers taxol resistance in ovarian cancer cells, 2) Delineate the mechanism of action by which MFAP5 decreases paclitaxel uptake by cancer tissue; and 3) Evaluate the efficacy of targeting MFAP5 in ovarian cancer treatment.
Program Official Information: Name: Wolfrey, Crystal; Phone: 240-276-6277; Email: wolfreyc@mail.nih.gov

R01 (Sun) 12/1/2018-11/30/2023 1.80 calendar
NIH/NIAID $250,000
Regulation of CD8 T Cell Responses and Antitumor Immunity by Otub1
Major goal(s): Investigate the role of a deubiquitinase (DUB), Otub1, in the regulation of IL-15R/TCR signaling and CD8 T cell responses.
Role: Principal Investigator
Specific Aim(s): 1) Define the mechanism by which Otub1 regulates AKT axis of IL-15 signaling and CD8 T cell homeostasis, 2) Elucidate the mechanism by which Otub1 regulates TCR signaling and antigen stimulated CD8 T cell responses; and 3) Examine the role of Otub1 in regulating CD8 T cell self-tolerance and antitumor immunity.
Program Official Information: Center for Scientific Review, National Institutes of Health, 6701 Rockledge Drive, Room 1040 - MSC 7710, Bethesda, MD 20892-7710; Phone: 301-435-0715

1R01CA226292-01A1 (Peng) 9/1/2018-8/31/2023 0.36 calendar
NIH/NCI $25,000
Characterize and Target the Mutator Phenotype in ARID1A-Deficient Ovarian Cancer
Major goal(s): Understand ARID1A's molecular functions and determine whether ARID1A deficiency can be exploited clinically for treatment of OCCC and for other tumors where ARID1A mutations are prevalent.
Role: Collaborator
Specific Aim(s): 1) Determine mechanism(s) by which ARID1A regulates mismatch repair, 2) Determine whether ARID1A deficiency confers a mutator phenotype in OCCC; and 3) Develop therapeutic approaches targeting ARID1A deficiency using immune checkpoint blockade.
Program Official Information: Name: Okano, Paul; Phone: 240-276-6250; Email: po8k@nih.gov

1R01CA231149-01 (Yu) 9/1/2018-8/31/2023 0.36 calendar
NIH/NCI $353,406
Combating Breast Cancer Brain Metastasis by Blocking the Two-Pronged Driver Kinase Function of CDK5
Major goal(s): Determine the brain metastasis-promoting functions of CDK5 in spontaneous brain metastasis models and in immune competent mouse models, and examine its clinical relevance in patient specimens.
Role: Co-Investigator
Specific Aim(s): 1) Determine the brain mets-promoting functions of CDK5 in spontaneous brain mets models and in immune competent mouse models, and examine its clinical relevance, 2) Explore novel mechanisms of CDK5-enhanced brain mets; and 3) Evaluate the potential of targeting CDK5 for early intervention and treatment of breast cancer brain mets.
Program Official Information: Name: Leota Hall; Phone: 240-276-6449; Email: leota.hall@nih.gov

1R01AI133822-01A1 (Watowich) 7/1/2018-6/30/2023 0.60 calendar
NIH/NIAID $268,376
Defining Protective Responses in Hematopoietic Cells Mediated by STAT3 Anti-Inflammatory Activity
Major goal(s): Provide novel insight into intrinsic HSPC protective mechanisms, fundamental information that will improve understanding of immune system regulation during inflammation.
Role: Co-Investigator
Specific Aim(s): 1) Investigate the cell intrinsic role for STAT3 in protecting hematopoietic function in inflammation; and 2) Delineate molecular pathways by which STAT3 protects HSCs from inflammation-induced damage.
Program Official Information: Name: Nasseri, M. Faraz; Phone: 240 627 3507; Email: fnasseri@niaid.nih.gov

1R01CA233596-01 (Liang) 9/1/2018-8/31/2022 0.60 calendar
NIH/NCI $292,580
Assessment and Benchmarking of Verteporfin Analogs for Potent and Selective Inhibition of PD-L1 in the Tumor Microenvironment
Major goal(s): Develop verteporfin analogs with sufficient drug potency and selectivity to target PD-L1 for cancer treatment.
Role: Co-Investigator
Specific Aim(s): 1) Synthesize verteporfin analogs and determine their relative potency and mechanisms to inhibit PD-L1 expression; and 2) Benchmarking of verteporfin analogs as an alternative approach to PD-L1 abrogation in a syngeneic setting.
Program Official Information: Venkatachalam, Sundaresan; Phone: 240-276-7304; Email: sundarv@nih.gov

(Mok) 8/31/2018-8/30/2022 1.20 calendar
CPRIT (Sub with Methodist Hospital Research Institute) $350,000
Targeting the Tumor Microenvironment Immune Response
Major goal(s): To have a significant impact on the development of new therapeutic strategies for ovarian cancer based on targeting the stromal-cancer cell crosstalk networks in ovarian tumor tissue.
Role: Co-Investigator
Specific Aim(s): 1) Generate transcriptome profiles from key stromal cell types in different ovarian tumor compartments, and from ovarian cancer cells at stromal-epithelial interface and at the center of tumor nests with high and low intraepithelial CD8+ CTL densities using immuno-laser microdissection and RNAseq, 2) Uncover differential crosstalk signaling networks among various cell types that are associated with decreased intraepithelial CD8+ CTL density and evaluate the effect of CAF specific gene perturbation on the networks and CD8+ T cell activation and trafficking; and 3) Use engineered exosomes to deliver siRNAs *in vivo* to target CAF-tumor crosstalk, and evaluate their effects on tumor progression and chemoresistance in HGSC animal models.
Program Official Information: 1701 North Congress Avenue, Suite 6-127, Austin, TX 78701; Phone: 512-463-3190; Email: cprit@cprit.state.tx.us

(Peng) 9/1/2018-8/31/2020 0.36 calendar
US Department of Defense (DoD) $184,885
Characterize and Target the Mutanome and Immunoresponsiveness in ARID1A-Deficient Gastric Cancer
Major goal(s): 1) Define a new role of the ARID1A-SWI/SNF chromatin remodeling complex in regulating MMR, 2) Gain novel insights into the mutanome/neoantigens resulted from ARID1A deficiency; and 3) Develop novel immune-based therapeutic strategies capitalizing on the mutanome-induced by ARID1A deficiency.
Role: Collaborator
Specific Aim(s): 1) Determine the functional importance of ARID1A-MSH2 interaction in regulating mismatch repair, 2) Characterize mutanome and its-associated neoantigens in ARID1A-deficient gastric cancer; and 3) Determine whether ARID1A deficiency induces TILs and activation of immune checkpoint in gastric cancer.
Program Official Information: 1077 Patchel Street, Fort Detrick, MD 21702-5024; Phone: 301-619-7071

OVERLAP
None.

Chi Lam Au Yeung, Ph.D.

Ongoing Research Support

Title: The FGF18/FGFR4 Amplicon: Novel Therapeutic Biomarkers for Ovarian Cancer
Funding agency: R01 CA169200-02, NIH/ NCI
Award dates: 2013/03/01-2019/02/28 (NCE)
Program officer: Kim, Kelly, Y. kimke@mail.nih.gov
PI: Mok, Samuel, Birrer, Michael
Goal: The major goal is to evaluate the functional role of FGF18 in ovarian cancer progression.
Specific aims:
Aim 1: To validate the prognostic value of FGF18/FGFR4 axis using a large collection of multi-center clinical trial specimens (GOG218)
Aim 2: To delineate the functional role and signaling network of FGF18 in ovarian tumor cells and ovarian tumor stromal cells in vitro and in vivo
Aim 3: To use the recently developed FGF trap proteins (from Five Prime Therapeutics Inc.) as proof of principle to target FGF18 as a novel therapeutic intervention against epithelial ovarian cancer.
Effort: 1.2 CM
Direct cost: $1,411,165
Role: Scientist

Title: The Genomic, Epigenomic and Psychosocial Characteristics of Long-Term Survivors of Ovarian Cancer.
Funding agency: W81XWH-16-2-0038, DOD
Award dates: 2016/09/30-2020/09/29
Program Officer: NA
PI: Birrer, Michael
Goal: The overall goal of this multi-institutional proposal is to enhance the understanding of the molecular, biologic and patient-reported outcome characteristics of long-term survivors of ovarian cancer.
Specific aims:
Aim 1: To study the genomic characteristics (in terms of micro RNA expression) of long-term versus short-term survivors of ovarian cancer.
Aim 2: Investigate the research data generated by other members of the consortium, predictive biomarkers for long-term ovarian cancer survival will be identified for better stratification and prognostication and more effective treatment of ovarian cancer patients.
Effort: 4.8 CM
Direct cost: $62,500
Role: Scientist

Title: The Role of Mesothelial Omentin in Ovarian Cancer Progression
Funding Agency: W81XWH-17-1-0146, DOD

Award dates: 2017/05/01-2020-04/30
Program officer: Dellinger, Susan M
PI: Yip, Daniel, Mok, Samuel
Goal: The overall goal of this proposal is to delineate the molecular mechanism by which omentin suppresses ovarian cancer progression
Specific aims:
Aim 1: Evaluate the mechanisms of action by which ITLN1 suppresses ovarian cancer cell motility and invasive potential.
Aim 2: Evaluate the mechanisms by which ITLN1 regulates ovarian cancer cell growth.
Aim 3: Evaluate the tumor suppressor role of ITLN1 in vivo and the efficacy of using ITLN1 in the treatment of ovarian cancer.
Effort: 4.8 CM
Direct cost: $45,000
Role: Scientist

Pending

None

Overlap

None

PREVIOUS, CURRENT, AND PENDING SUPPORT

Wong, Stephen

PREVIOUS

Title: Assisted follow-up in neuroimaging of therapeutic intervention
Time Commitment: N/A
Funding Agency: NIH, G08LM008937
Agency Contact and Address: Andrew Diggs, diggsa@mail.nih.gov, 301-451-4238
Performance Period: 04/01/2007-03/31/2012
Funding Level: $147,227 per year
Role: PI
Goals and Aims: To develop an integrated computer aided diagnosis and informatics system to aid the quantitative following up and monitoring of brain tumor patients.
Overlap: No overlap

Title: High-content image analysis and modeling for neuron assay based screening
Time Commitment: N/A
Funding Agency: NIH, R01AG028928-01A1
Agency Contact and Address: Richard Proper, proper@mail.nih.gov, 301-402-7735
Performance Period: 09/15/2007-06/30/2012
Funding Level: $344,609 total per year
Role: PI
Goals and Aims: To develop a high content neurite outgrowth imaging screening pipeline to screen small molecules for Alzheimer's disease.
Overlap: No overlap

Title: Life Science systems and applications conference
Time Commitment: N/A
Funding Agency: NLM/NIH, R13LM009571
Agency Contact and Address: Ebony Simmons, 301-594-4917
Performance Period: 08/01/2007-7/30/2012
Funding Level: $18,849 total per year
Role: PI
Goals and Aims: To organize an interdisciplinary workshop involving engineers, biologists, and clinicians in exchanging ideas of the latest development in life science advances.
Overlap: No overlap

Title: Neuronal spines tracking and analysis for time-lapse, 3D optical microscopy
Time Commitment: N/A
Funding Agency: NLM/NIH, R01LM009161
Agency Contact and Address: Dwight Mowery, moweryd@mail.nlm.nih.gov, 301-496-4221
Performance Period: 09/15/2007-06/30/2012
Funding Level: $333,098 total per year
Role: PI

Goals and Aims: To develop new computational tools to track and analyze 3D confocal images of tissue-cultured neurons in order to understand dynamic and quantitative models of spine morphology in neurodegenerative diseases.
Overlap: No overlap

Title: A multimodality image-guided system for peripheral lung cancer diagnosis and therapy
Time Commitment: N/A
Funding Agency: CPRIT, RP100627
Agency Contact and Address:
Performance Period: 03/01/2010-02/28/2013
Funding Level: $360,000 direct per year
Role: PI
Goals and Aims: Development of a minimally invasive multimodality image guided system for early diagnosis and treatment of peripheral lung cancer, by integrating macroscopic and microscopic imaging, fiberoptic fluorescence molecular imaging, and electromagnetic tracking based intervention in one platform via user friendly 3D visualization and navigation.
Overlap: No overlap

Title: Center for Systematic Modeling of Cancer Development
Time Commitment: N/A
Funding Agency: NIH/NCI, U54 CA149196
Agency Contact and Address: Dan Gallahan, 240-276-6180
Performance Period: 03/01/2010-02/28/2015
Funding Level: $1,996,952 direct per year
Role: PI
Goals and Aims:
1.1: To identify tumor-initiatinc cells using newly developed lentiviral fluorescent signaling reporters and to characterize their spatial distribution and behaviors during tumor growth using in vivo imaging.
1.2: To identify candidate genes and pathways that may regulate TIC behaviors.
1.3: To conduct a "Directed Iterative Functional Genomic Screen" to characterize genes functionally that either increase or decrease tumor-initiating capacity.
1.4: To define the cellular responses of TIC to genetic and pharmacological manipulation of genes regulating TIC survival or function in vivo.
2.1: To model the TIC tissue mE mathematically based on 2D and 3D microscopy and image analysis.
2.2: To predict the TIC pathways or key genes related to specific cancer subtypes so to refine the TIC microenvironment model.
2.3: To develop bioimaging informatics models for mapping gene functional networks within and among TIC and niche cells from the directed iterative shRNA screen and further refine the TIC mE model.
2.4: To model the response of TIC and their microenvironment to genetic and pharmacological manipulations of TIC function in vivo.
Overlap: No overlap

Title: A label-Free and Chemical-Selective Microendoscope To Enhance Prostate Surgical Outcomes
Time Commitment: N/A
Funding Agency: DOD, PC111860
Agency Contact and Address: Kathy E. Robinson, 301-682-5507
Performance Period: 09/30/2012-09/29/2015
Funding Level: $124,480 direct per year
Role: PI
Goals and Aims:
1. To refine the existing CARS microendoscope into an all-fiber device for *in vivo* cancer imaging.
2. To evaluate the ability of our CARS microendoscope to image cavernous nerves and prostate surgical margins *in vivo* using intrinsic CH2-based molecular contrast.
Overlap: No overlap

Title: High content image analysis and modeling for RNAi genome-wide screening
Time Commitment: N/A
Funding Agency: NIH/NCI, R01 CA121225
Agency Contact and Address: Jennifer Couch, 240-276-6210
Performance Period: 09/30/2008–08/30/2014
Funding Level: $311,274 total per year
Role: PI
Goals and Aims:
To develop new cell-based assay and associated analytic tool for analyzing and modeling genome-wide RNAi screening for Rho family of proteins.
Overlap: No overlap

Title: Data Analysis – Collaborative Research and Support from Bioinformatics Core
Time Commitment: N/A
Funding Agency: RP101334, CPRIT Gulf Coast Consortia High-throughput Screening Program
Agency Contact and Address: Lisa Nelson, 512-305-8418
Performance Period: 05/01/2010-05/01/2016
Funding Level: $398,000
Role: Core-PI: Wong
Goals and Aims: (Bioinformatics)
The Bioinformatics Core will actively interact with screening programs and investigators to well understand the project purpose, collect related supporting data, satisfy the data analysis needs of screening projects, and perform integrative and systemic data analysis to provide bioinformatics clues for experimental design of focused and combinatorial screening projects, selection of true positive hits, secondary experimental design, and interpretation of mechanism of action.
Overlap: No overlap

Title: Mobile Multi-Modal Label-Free Imaging Probe Analysis of Chorodial Oximetry and Retinal Hypoxia
Time Commitment: N/A
Funding Agency: MR130311, DOD Vision Research Program

Agency Contact and Address: Jessica Clement, 301-619-4047
Performance Period: 09/30/2014-09/29/2016
Funding Level: $88,502
Role: PI
Goals and Aims:
1. Create PBI animal model and develop and calibrate the mobile, optical fiber-based CARS microendoscope probe to measure oxy-hemoglobin content in the eye.
2. Detect and map hypoxic regions in injured, PBI eyes using the mobile microendoscope probe.
3. Measure TRPM7 biomarker in mapped hypoxic eye regions.
4. Analyze and evaluate TRPM7 activity in both normal and injured eyes using biochemistry and electrophysiology.
Overlap: No overlap

CURRENT

Title: Modeling tumor-stroma crosstalk in lung cancer to identify targets for therapy
Time Commitment: 15% FTE
Funding Agency: 1U01CA188388-01A1, NCI/NIH
Agency Contact and Address: Brian Iglesias, (240) 276-6278
Performance Period: 07/01/2015-06/30/2019
Funding Level: $484,162
Role: MPI Wong, Mittal
Goals and Aims:
1. To develop and improve the multi-cellular network for uncovering tumor-stroma crosstalk signaling pathways.
2. To identify tumor-stroma crosstalk signaling networks in NSCLC.
3. To evaluate the therapeutic potential of tumor-stroma crosstalk in NSCLC.
Overlap: No overlap

Title: Ting Tsung and Wei Fong Chao Center for Bioinformatics Research and Imaging for Neurosciences (BRAIN)
Time Commitment: 15% FTE
Funding Agency: Chao Foundation
Agency Contact: N/A
Performance Period: 1/1/2010-12/31/2019
Funding Level: $300,000 per year
Role: PI
Goals and Aims: The goal is to translate research findings into clinical therapies quickly and effectively using a variety of approaches including computational analysis, biomedical imaging, molecular modeling, genetic analysis, pre-clinical models, and clinical studies.
Overlap: No overlap.

Title: Genetic mechanisms of Alzheimer's Disease associated with Environmental Metal Exposure
Time Commitment: 5% FTE
Funding Agency: 5R01ES024165-04S1, NIH

Agency Contact: Anette Kirshner, kirshner@niehs.nih.gov
Performance Period: 07/01/2017-04/30/2019
Funding Level: $80,000
Role: Co-investigator (PI: Weisskopf)
Goals and aims: Our contribution to this effort is Specific Aim 3, in which we determine SNP/copy number variation related to the target genes in whole genome sequences of 10 subjects, and determine whether any of these changes are also found in the ADNI database.
Overlap: No overlap

PENDING

Title: DrugComboExplorer: Precision Drug Combinations Using Pharmacogenomics Big Data and Electronic Medical Records
Time Commitment: 20% FTE
Funding Agency: R01LM12588-01A1, NIH
Agency Contact: Joseph Rudolph, 301-408-9098
Performance Period: 7/1/18-6/30/23
Funding Level: $250,000 per year
Role: PI
Goals and aims: We aim to create a predictive analytics tool, DrugComboExplorer (DCE), by integrating large scale genomic, transcriptomic, pharmacogenomic, and phenotypic data sets generated by NIH-funded initiatives (the Cancer Genome Atlas - TCGA, Library of Integrated Network-Based Cellular Signatures - LINCS, Therapeutically Applicable Research To Generate Effective Treatments – TARGET, and the database of Genotypes and Phenotypes - dbGaP) and our in-house enterprise data warehouse of electronic medical records (EMR). DCE computes the signaling networks for each cancer sample, outputs potential drug combination treatment tailored to an individual patient, and evaluates the risk of adverse events from the drugs. The resulting precision drug combination should reduce the risk of drug resistance and toxicity.
Overlap: No overlap

Title: Systematic Alzheimer's disease drug repositioning (SMART) based on bioinformatics-guided phenotype screening and image-omics
Time Commitment: 20% FTE
Funding Agency: R01AG057635-01A1, NIH
Agency Contact: Alexander Parsadanian, 301-402-7708
Performance Period: 7/1/18-6/30/23
Funding Level: $430,269
Role: PI
Goals and aims:

1. To develop a systematic AD drug repositioning framework that integrates bioinformatics-guided phenotype screening and advanced bioinformatics analytics.
2. To construct an image-omics workflow to uncover the molecular mechanism underlying compounds that block AD pathogenic events.
3. In vitro and in vivo validation of the identified repositioned drugs.

Overlap: No overlap

Title: Predicting and targeting exosome-mediated crosstalk in ovarian cancer microenvironment
Time Commitment: 25% FTE
Funding Agency: U01CA232151, NCI/NIH
Agency Contact: Shannon Hughes, 240-276-6224
Performance Period: 7/1/18-6/30/23
Funding Level: $383,003
Role: MPI
Goals and aims:

1. Develop computational modeling methods to identify exosome-mediated crosstalk between HGSC cells and CAF or CAA, and determine the role of CAF- and CAA-derived exosomes on tumor progression and chemoresistance.
2. Identify the receptor-based signaling pathways in HGSC cells modulated by CAF- and CAA-derived exosomal ncRNA-mediated pathways.
3. Identify therapeutic agents that target stromal-derived ncRNAs and major signaling pathways, and evaluate their effects in tumor progression and chemoresistance in HGSC animal models.

Overlap: no overlap

Title: Ovarian Cancer Human Tumor Atlas: cellular and molecular 3D reconstruction
Time Commitment: 25% FTE
Funding Agency: U2CCA233299, NCI/NIH
Agency Contact: Shannon Hughes, 240-276-6224
Performance Period: 09/01/2018-08/31/2023
Funding Level: $611,687
Role: Project PI (PI: Mok)
Goals and aims: The proposed Ovarian Cancer Human Tumor Atlas Research Center (OCHTARC) will construct an atlas describing (1) the development of therapeutic resistance, and (2) the dynamic response to chemotherapy in advanced stage ovarian cancer. Three dimensional (3D) mapping of cellular and molecular contents in primary and recurrent tumors obtained from multiple metastatic sites in patients with high-grade serous ovarian cancer will be performed using multiple analytical validated platforms.
Overlap: no overlap

Title: Targeting Tumor Microenvironment Immune Response (TuMIR)
Time Commitment: 30% FTE
Funding Agency: CPRIT RP180853
Agency Contact: Richard Kolodner, 512-305-8491
Performance Period: 08/31/2018-08/30/2022
Funding level: $1,362,394
Role: PI
Goals and aims:

1. To use innovative computational approaches to identify cancer-stromal cell molecular crosstalk that mediates altered immune response in the ovarian tumor microenvironment.

2. To evaluate the clinical relevance of the key crosstalk signaling and experimentally determine the effects of perturbing identified cancer/stromal crosstalk networks on the tumor immune response.
3. To develop a novel engineered exosomes system and reposition existing drugs or drug combinations to facilitate tumor immune response.

Overlap: no overlap

Title: Deep Pathways Learning for Disease Modeling
Time Commitment: 15% FTE
Funding Agency: R21LM013028-01, NLM/NIH
Agency Contact: Jane Ye, 301-594-4927
Performance Period: 09/01/2018-08/31/2020
Funding Level: $125,000
Role: PI
Goals and aims:

1. Investigate and model cancer pathway's impact on patients' survival.
2. Explicitly model the combined effects of gene expression, methylation, mutation, and copy number variation data based on the same gene symbol as a gene effect module.

Overlap: no overlap

Title: Systematic Alzheimer's disease therapeutic design using zebrafish-based smart screening platform
Time Commitment: 20% FTE
Funding Agency: R01AG061392, NIH
Agency Contact: Robin Barr, 301-496-9322
Performance Period: 09/01/2018-08/31/2023
Funding Level: $372,136
Role: MPI
Goals and aims:

1. To identify individual gamma-secretase substrate-derived ICDs that suppress neuron/axon loss in stable gamma-secretase-deficient zebrafish.
2. To automate image acquisition of zebrafish expressing ICDs and establish phenomics of stable gamma-secretase deficient zebrafish.
3. To predict and validate combination ICD treatment preventing neuronal loss in zebrafish.

Overlap: no overlap

8. SPECIAL REPORTING REQUIREMENTS

Nothing to report

9. APPENDICES

Leung CS, Yeung TL, Yip KP, Wong, KK, Ho SY, Mangala LS, Sood AK, Lopez-Berestein G, Sheng J, Wong ST, Birrer MJ, Mok SC. Cancer-associated fibroblasts regulate endothelial adhesion protein LPP to promote ovarian cancer chemoresistance. J Clin Invest. 2018;128(2):589-606. PubMed PMID: 29251630; PubMed Central PMCID:PMC5785271.

Cancer-associated fibroblasts regulate endothelial adhesion protein LPP to promote ovarian cancer chemoresistance

Cecilia S. Leung,[1,2] Tsz-Lun Yeung,[1] Kay-Pong Yip,[3] Kwong-Kwok Wong,[1,2] Samuel Y. Ho,[1] Lingegowda S. Mangala,[1,4,5] Anil K. Sood,[1,4,5] Gabriel Lopez-Berestein,[4,5,6] Jianting Sheng,[7,8] Stephen T.C. Wong,[7,8] Michael J. Birrer,[9] and Samuel C. Mok[1,2]

[1]Department of Gynecologic Oncology and Reproductive Medicine, The University of Texas MD Anderson Cancer Center, Houston, Texas, USA. [2]The University of Texas Graduate School of Biomedical Sciences at Houston, Houston, Texas, USA. [3]Department of Molecular Pharmacology and Physiology, University of South Florida, Tampa, Florida, USA. [4]Department of Cancer Biology, [5]The Center for RNA Interference and Non-Coding RNAs, and [6]Department of Experimental Therapeutics, The University of Texas MD Anderson Cancer Center, Houston, Texas, USA. [7]Department of Systems Medicine and Bioengineering, and [8]NCI Center for Modeling Cancer Development, Houston Methodist Research Institute, Houston, Texas, USA. [9]Comprehensive Cancer Center, Division of Hematology-Oncology, University of Alabama at Birmingham, Birmingham, Alabama, USA.

The molecular mechanism by which cancer-associated fibroblasts (CAFs) confer chemoresistance in ovarian cancer is poorly understood. The purpose of the present study was to evaluate the roles of CAFs in modulating tumor vasculature, chemoresistance, and disease progression. Here, we found that CAFs upregulated the lipoma-preferred partner (*LPP*) gene in microvascular endothelial cells (MECs) and that *LPP* expression levels in intratumoral MECs correlated with survival and chemoresistance in patients with ovarian cancer. Mechanistically, *LPP* increased focal adhesion and stress fiber formation to promote endothelial cell motility and permeability. siRNA-mediated *LPP* silencing in ovarian tumor–bearing mice improved paclitaxel delivery to cancer cells by decreasing intratumoral microvessel leakiness. Further studies showed that CAFs regulate endothelial *LPP* via a calcium-dependent signaling pathway involving microfibrillar-associated protein 5 (MFAP5), focal adhesion kinase (FAK), ERK, and LPP. Thus, our findings suggest that targeting endothelial LPP enhances the efficacy of chemotherapy in ovarian cancer. Our data highlight the importance of CAF–endothelial cell crosstalk signaling in cancer chemoresistance and demonstrate the improved efficacy of using LPP-targeting siRNA in combination with cytotoxic drugs.

Introduction

High-grade serous ovarian cancer (HGSC) is the most common histological subtype of ovarian cancer and accounts for most ovarian cancer–related deaths. Most HGSCs are diagnosed at a late stage, and, as a result, the overall survival rate of patients with HGSC is less than 30%. The clinical biological characteristics of HGSC suggest that late diagnosis and the persistence of drug-resistant cancer cells limit our ability to cure this disease.

Tumor vasculature plays an important role in the pathogenesis and progression of HGSC and is crucial in modulating the delivery of therapeutic agents (1). Various tumor cell–derived cytokines, including VEGFs and FGFs, are involved in HGSC pathogenesis and progression. Although phase I and II trials of the VEGF-α–targeting monoclonal antibody bevacizumab in patients with ovarian cancer yielded encouraging results, phase III trials of the drug as a frontline treatment for ovarian cancer patients (Gynecologic Oncology Group 218 [GOG 218] and International Collaboration on Ovarian Neoplasms 7 [ICON7]) and recurrent ovarian cancer (Ovarian Cancer Study Comparing Efficacy and Safety of Chemotherapy and Anti-Angiogenic Therapy in Platinum-Sensitive Recurrent Disease [OCEANS] and Avastin Use in Platinum-Resistant Epithelial Ovarian Cancer [AURELIA]) have demonstrated that bevacizumab yields only a modest improvement in progression-free survival and no significant improvement in overall survival (2–5). These findings suggest that other proangiogenic mediators and pathways compensate for VEGF blockade and allow angiogenesis to occur, despite anti-VEGF therapy (1). Further research, including that aimed at identifying new proangiogenic targets and markers to optimize patient selection, is essential to maximize the potential of antiangiogenic therapy for ovarian cancer.

Cancer-associated fibroblasts (CAFs), one of the primary stromal cell types in ovarian tumor tissues (6), secrete CAF-specific proteins, cytokines, and growth factors and produce an extracellular matrix (ECM) that supports tumor cell growth and angiogenesis and confers chemoresistance (7–11). However, the mechanisms by which CAFs promote angiogenesis in ovarian cancer remain poorly understood. In addition, few studies have sought to identify CAF-derived mediator–regulated endothelial biomarkers that are associated with chemoresistance. We searched for CAF-regulated proangiogenic effector molecules in microvascular endothelial cells (MECs) and identified elevated expression of the lipoma-pre-

Authorship note: C.S. Leung and T.L. Yeung are co–first authors.
Conflict of interest: The authors have declared that no conflict of interest exists.
Submitted: May 17, 2017; **Accepted:** November 7, 2017.
Reference information: *J Clin Invest*. 2018;128(2):589–606.
https://doi.org/10.1172/JCI95200.

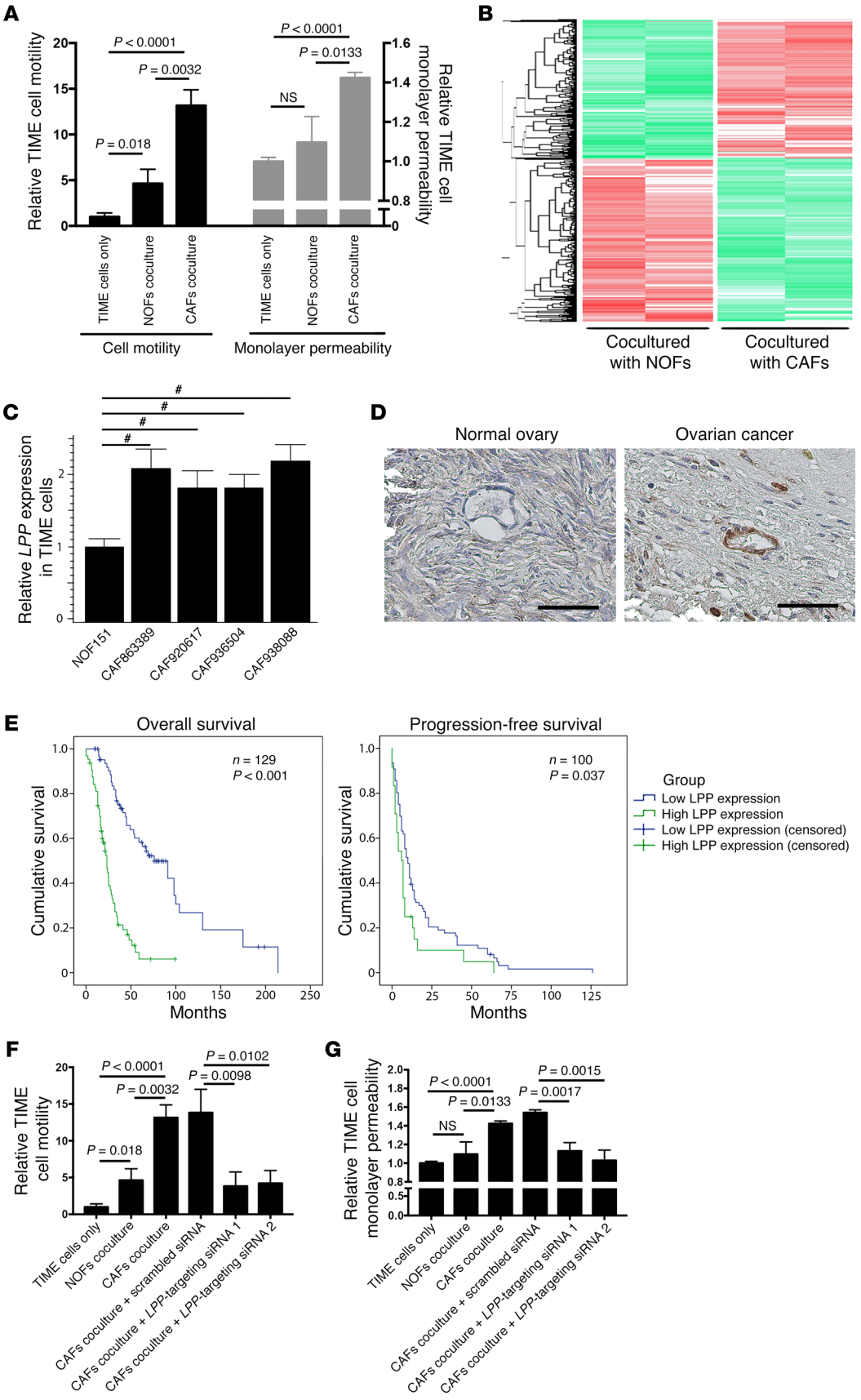
A
Relative TIME cell motility
Relative TIME cell monolayer permeability
P < 0.0001
P = 0.0032
P = 0.018
P < 0.0001
P = 0.0133
NS
TIME cells only
NOFs coculture
CAFs coculture
Cell motility
Monolayer permeability
B
Cocultured with NOFs
Cocultured with CAFs
C
Relative LPP expression in TIME cells
NOF151
CAF863389
CAF920617
CAF936504
CAF938088
D
Normal ovary
Ovarian cancer
E
Overall survival
n = 129
P < 0.001
Progression-free survival
n = 100
P = 0.037
Cumulative survival
Months
Group
Low LPP expression
High LPP expression
Low LPP expression (censored)
High LPP expression (censored)
F
Relative TIME cell motility
P = 0.0102
P = 0.0098
CAFs coculture + scrambled siRNA
CAFs coculture + LPP-targeting siRNA 1
CAFs coculture + LPP-targeting siRNA 2
G
Relative TIME cell monolayer permeability
P = 0.0015
P = 0.0017

Figure 1. CAF-induced endothelial LPP expression in ovarian cancer. (**A**) TIME MECs cocultured with CAFs had significantly higher motility rates and monolayer permeability compared with MECs cocultured with NOFs. *P* values were determined by 2-tailed Student's *t* test. (**B**) Heatmap generated from transcriptome analyses of RNA samples isolated from TIME cells cocultured with CAFs or NOFs. A total of 1,394 genes and 2,106 genes were up- and downregulated, respectively, in TIME cells cocultured with CAFs versus MECs cocultured with NOFs (fold change >1.5; Benjamini-Hochberg multiple testing–adjusted $P < 0.05$). LPP was identified as one of the significantly upregulated genes. (**C**) Quantitative reverse transcription PCR (qRT-PCR) analyses of endothelial cells RNA samples confirmed that endothelial LPP expression was upregulated in the presence of CAFs ($^{\#}P < 0.0001$, by 2-tailed Student's *t* test). (**D**) Hematoxylin-counterstained images of immunolocalization of LPP in a normal ovary and a high-grade serous ovarian cancer showing that ovarian tumor MECs had higher LPP expression levels than did normal ovarian MECs. Scale bars: 50 μm. (**E**) Kaplan-Meier analysis were used to evaluate the clinical relevance of endothelial LPP expression in patients with HGSC. Elevated endothelial LPP expression was associated with lower overall and progression-free survival. The median overall survival rate of HGSC patients with high endothelial LPP levels (23 months) was significantly shorter than that of patients with low endothelial LPP levels (76 months) ($n = 129$; $P < 0.001$, by log-rank test). The median progression-free survival rate duration of HGSC patients with high endothelial LPP levels (6 months) was significantly shorter than that of patients with low endothelial LPP levels (10 months) ($n = 100$; $P < 0.037$, by log-rank test). (**F**) CAFs increased endothelial cell motility, and the motility-promoting effect of CAFs was attenuated in endothelial cells transfected with LPP-targeting siRNAs. Motility assays were performed using Boyden chambers. Endothelial cells in the upper chamber were allowed to migrate through the porous membrane in the presence of CAFs or NOFs in the bottom chamber (*P* values were determined by 2-tailed Student's *t* test). (**G**) CAFs increased the permeability of a confluent endothelial cell monolayer, and the permeability-enhancing effect of CAFs was attenuated in endothelial cells transfected with LPP-targeting siRNAs (*P* values were determined by 2-tailed Student's *t* test). Fluorescence-labeled dextran was added to a confluent monolayer culture of endothelial cells in the upper chamber of a Boyden chamber and the amount of dextran diffusing through the endothelial cell monolayer culture in the presence of CAFs or NOFs to the lower chamber was measured by an ELISA microplate reader. All data represent the mean ± SEM of 3 independent experiments.

ferred partner (*LPP*) gene in MECs cocultured with CAFs. *LPP* is a member of a subfamily of LIM domain proteins that are characterized by an N-terminal protein–rich region and 3 C-terminal LIM domains (12, 13). It mainly localizes to the cell periphery in focal adhesion and is involved in cell-cell adhesion, cell-substrate cytoskeletal interactions, and cell motility in Madin-Darby canine kidney (MDCK) epithelial cells (14). In addition, LPP has been shown to bind to LASP1, which enhances the motility of embryonic fibroblasts (15). The roles of endothelial LPP in tumor angiogenesis and in conferring chemoresistance have not been reported to date.

The purpose of the present study was to evaluate the roles of CAFs in modulating tumor vasculature and disease progression. On the basis of our experimental results, we found elevated levels of *LPP* expression in MECs in the presence of CAFs and demonstrated the prognostic significance of endothelial LPP in patients with HDSC. We also delineated the molecular mechanism by which *LPP* increases microvascular endothelial cell motility and leakiness and decreases the delivery of paclitaxel to tumors in vivo. Furthermore, using murine models, we showed that *LPP* silencing inhibits ovarian tumor growth and improves paclitaxel bioavailability by reducing intratumoral microvessel leakiness. Finally, we demonstrated that CAF-derived microfibrilla–associated protein 5 (MFAP5) can upregulate *LPP* in MECs via a calcium-dependent MFAP5/FAK/ERK/LPP signaling pathway.

Results

CAFs upregulate LPP in MECs. The ovarian tumor microenvironment, which is composed primarily of fibroblasts, ECM proteins, endothelial cells, and lymphocytic infiltrates, can regulate tumor growth, angiogenesis, dissemination, and chemoresistance (11, 16). CAFs have been shown to play crucial roles in cancer progression. Although increasing evidence demonstrates that CAFs have important roles in modulating the aggressive phenotypes of cancer cells, their effects on the tumor vasculature remain underexplored. We cocultured human telomerase-immortalized microvascular endothelial (TIME) cells with either primary human ovarian CAFs or normal ovarian fibroblasts (NOFs) to evaluate the effects of CAFs on endothelial cell motility and monolayer permeability. We found that TIME cells that had been cocultured with CAFs had significantly higher rates of motility and monolayer permeability than did those cocultured with NOFs (Figure 1A).

To determine the underlying molecular mechanism by which CAFs promote angiogenesis, we performed a transcriptome analysis of RNA samples isolated from TIME cells that had been cocultured with CAFs or NOFs. We identified 1,394 genes and 2,106 genes that were up- and downregulated, respectively, in TIME cells cocultured with CAFs compared with those cocultured with NOFs (fold change >1.5, Benjamini-Hochberg multiple testing–adjusted $P < 0.05$) (Figure 1B and Supplemental Table 1; supplemental material available online with this article; https://doi.org/10.1172/JCI95200DS1). To uncover the biological functions of the CAF-induced gene expression profile in TIME cells, we used Ingenuity Pathway Analysis (IPA) software to analyze the list of genes that were upregulated in TIME cells cocultured with CAFs. Among the top 15 predicted activated biological functions, 10 are related to cell motility, invasion potential, and cytoskeleton organization (Table 1), which suggests that CAFs play an important role in the mobility of endothelial cells. Since increased endothelial cell motility can facilitate angiogenesis, we examined the list of genes identified by IPA that had the highest ranked cell movement–related function (activation *Z* score = 6.943; $P = 9.49 \times 10^{-28}$). We selected LPP, a LIM domain–containing protein that interacts with the cytoskeleton, for further validation studies. As a cell motility regulatory protein, the roles of LPP in angiogenesis, chemoresistance, and tumor progression have not been investigated. We first performed a quantitative reverse transcription PCR (qRT-PCR) analysis using RNA samples isolated from endothelial cells cocultured with CAFs or NOFs and found that *LPP* mRNA was upregulated in TIME cells cocultured with CAFs compared with levels in those cocultured with NOFs (Figure 1C).

LPP overexpression is associated with poor survival rates and increased fibrosis in patients with HGSC. Blood vessels in tumor tissue are usually poorly organized and leaky, which impairs drug delivery (17). Because *LPP* has been shown to be involved in cell-cell adhesion, cell-substrate cytoskeletal interactions, and cell motility (14), we hypothesized that the CAF-induced upregulation

Table 1. Predicted biological functions of the CAF-induced gene expression profile in TIME cells

Rank	Function	*P* value	Predicted activation state	Activation *Z* score
1	Size of body	7.56×10^{-09}	Increased	10.567
2	Cell survival	5.75×10^{-13}	Increased	7.977
3	Cell viability	5.72×10^{-12}	Increased	7.830
4	Cell movement	9.49×10^{-28}	Increased	6.943
5	Homing of cells	2.74×10^{-08}	Increased	6.905
6	Cell viability of tumor cell lines	2.66×10^{-08}	Increased	6.749
7	Chemotaxis	8.23×10^{-09}	Increased	6.540
8	Migration of cells	1.10×10^{-24}	Increased	6.412
9	Invasion of cells	1.82×10^{-21}	Increased	6.322
10	Organization of cytoplasm	1.92×10^{-19}	Increased	6.183
11	Organization of cytoskeleton	6.28×10^{-18}	Increased	6.183
12	Invasion of tumor cell lines	1.12×10^{-18}	Increased	6.170
13	Formation of cellular protrusions	2.66×10^{-13}	Increased	6.095
14	Cell movement of tumor cell lines	5.14×10^{-17}	Increased	6.082
15	Microtubule dynamics	4.24×10^{-12}	Increased	5.427

of LPP in endothelial cells in HGSC increases microvascular leakiness, thus decreasing the bioavailability of drugs such as paclitaxel to tumor cells. To test this hypothesis, we first performed immunolocalization of LPP in 10 normal ovarian and 129 HGSC tissue samples. Compared with those in normal ovarian tissue, the endothelial cells and surrounding smooth muscle cells in HGSC samples had a substantially higher LPP expression level (Figure 1D). Next, we determined the prognostic significance of endothelial LPP in HGSC. A Kaplan-Meier analysis and log-rank tests showed that high endothelial LPP expression was associated with lower overall and progression-free survival rates than was low endothelial LPP expression (Figure 1E), suggesting that endothelial LPP plays a role in ovarian cancer progression and chemoresistance.

Since the presence of CAFs is associated with tumor tissue fibrosis and our data showed that endothelial LPP expression was upregulated by coculturing MECs with CAFs, we determined whether there was a correlation between endothelial LPP expression and the degree of fibrosis. We performed Picrosirius red staining for collagen on 24 HGSC tissue samples expressing high or low levels of endothelial LPP. Collagen staining results demonstrated that HGSC patients with high expression levels of endothelial LPP had significantly higher collagen coverage and density than did patients with low expression levels of endothelial LPP (Supplemental Figure 1), suggesting an increase in fibrosis in tumor tissue with higher endothelial LPP expression.

LPP increases endothelial cell motility and monolayer permeability. To assess the effects of CAFs in upregulating LPP to promote endothelial cell motility, we subjected TIME MECs to motility assays using Boyden chambers, in which endothelial cells in the upper chamber were allowed to migrate through the porous cell culture membrane in the presence of CAFs or NOFs in the bottom chamber. We observed that CAFs enhanced endothelial cell motility, and the motility-promoting effect of CAFs was attenuated in endothelial cells transfected with *LPP*-targeting siRNAs (Figure 1F). These data suggest that endothelial LPP mediates the effect of CAFs on enhancing the motility potential of endothelial cells.

To determine whether *LPP* mediates the effect of CAFs in modulating endothelial cell permeability, we added fluorescence-labeled dextran to a confluent monolayer culture of endothelial cells in the upper chamber of a Boyden chamber and then allowed dextran to diffuse through the culture and the porous cell membrane in the presence of CAFs or NOFs in the lower chamber. The fluorescent signal in the lower-chamber media that contained CAFs was significantly higher than that of the media that contained NOFs, suggesting that CAFs enhanced the permeability of the endothelial cell monolayer. This permeability-enhancing effect was attenuated in endothelial cells transfected with *LPP*-targeting siRNAs. These data suggest that LPP mediates the effect of CAFs in increasing the permeability of the endothelial cell monolayer (Figure 1G).

We compared the proliferation rates of parental and LPP-silenced endothelial cells using WST-1 cell proliferation assays. The experimental results showed that endothelial cell proliferation was not significantly affected by LPP silencing (Supplemental Figure 2), suggesting that LPP-induced endothelial cell migration in Boyden chambers and monolayer permeability are independent of cell proliferation.

LPP silencing increases paclitaxel uptake and suppresses tumor growth in vivo. The results of our in vitro studies of *LPP* silencing suggest that *LPP* mediates the effect of CAFs in facilitating tumor angiogenesis and enhancing tumor vessel leakiness, which may subsequently reduce the uptake of chemotherapeutic agents by cancer cells. To determine the roles of *LPP* in tumor progression and chemoresistance in vivo, we treated OVCA432 ovarian tumor–bearing mice twice weekly with tail-vein injections of chitosan nanoparticles incorporated with 5 μg control scrambled siRNA, murine *Lpp*–targeting siRNA 1, or murine *Lpp*–targeting siRNA 2 in combination with weekly i.p. injections of either sterile PBS or paclitaxel (3.5 mg/kg) for 6 weeks. All mice in all treatment groups were euthanized at the experimental endpoint. We harvested and weighed the i.p. tumor nodules and found that endothelial *Lpp* expression in tumor tissues from mice treated with *Lpp*-targeting siRNAs was markedly lower than that in tumor tissues from mice treated with scrambled siRNA (Figure 2A). Furthermore, mice treated with *Lpp*-targeting siRNA 1 or siRNA 2 had significantly smaller tumor burdens than did mice treated with scrambled siRNA ($P = 0.0048$ and $P = 0.0008$, respectively) (Figure 2B). Immunolocalization of tumor vessels by CD31 staining revealed that the microvessel densities in the *Lpp*-silenced groups were lower than those in the control group (Figure 2C), suggesting that *Lpp* silencing suppresses tumor angiogenesis and cancer progression.

Next, we determined whether *Lpp* silencing can increase paclitaxel delivery to ovarian cancer cells through tumor vessel normal-

ization and promote the treatment efficacy of paclitaxel in ovarian tumor–bearing mice. For each of the aforementioned siRNA treatment groups, we injected half the mice with FITC-dextran via the tail vein 1 hour before euthanasia to evaluate tumor vessel leakiness and injected the other half with Oregon Green 488 fluorescence–labeled paclitaxel via the tail vein 1 hour before euthanasia to evaluate drug delivery within the tumor tissue. As expected, among the mice injected with the scrambled siRNA, the tumor burden in mice treated with paclitaxel was significantly smaller than that in mice treated with PBS ($P = 0.0107$). In addition, the tumor weights in the paclitaxel-treated mice injected with either *Lpp*-targeting siRNA was significantly smaller than tumor weights in mice injected with scrambled siRNA ($P = 0.0055$ and $P = 0.0005$) (Figure 2B), suggesting that Lpp confers paclitaxel resistance in these mice.

Fluorescence microscopy was used to visualize FITC-dextran and Oregon Green 488 green fluorescence–labeled paclitaxel in frozen tissue sections prepared from tumor nodules harvested from the different treatment groups. Compared with those from control mice, ovarian tumor tissues from mice treated with *Lpp*-targeting siRNA had a markedly lower FITC-dextran signal (Figure 2D). Because dextran, which has a molecular weight of 70,000 kDa, can pass through only the endothelial cell layer of leaky tumor vessels, the lower FITC-dextran signal in the tumors from mice treated with *Lpp*-targeting siRNA suggests that Lpp silencing decreases vessel leakiness in the tumor tissue of these mice. The fluorescence-labeled paclitaxel signal in ovarian tumor tissues harvested from mice treated with *Lpp*-targeting siRNA was substantially higher than that in tumor tissues from control mice (Figure 2E), suggesting that *Lpp* silencing promotes the delivery of paclitaxel via blood vessels to cancer cells and subsequently increases the bioavailability of the agent to cancer cells in these mice.

CAF-derived MFAP5 upregulates endothelial LPP expression. To identify CAF-derived mediators that modulate LPP expression in MECs, we first examined the promoter sequence of *LPP*. We found that this sequence has multiple AP1-binding sites, which suggests that LPP expression can be regulated by the c-Fos/c-Jun transcriptional complex (Supplemental Figure 3). By querying the IPA database, we obtained a list of upstream ligands that have been shown to activate c-Fos/c-Jun signaling pathways. By comparing the IPA ligand list with our information on upregulated secretory ligands identified in CAFs (8), we generated a list of secretory ligands that were overexpressed in CAFs compared with expression in NOFs and that have been shown to activity c-Fos/c-Jun (Supplemental Table 2). Among them, MFAP5 was selected for further validation studies, because MFAP5 has recently been shown to be a CAF-derived mediator that can promote ovarian cancer cell motility through the c-Jun signaling cascade and because stromal MFAP5 overexpression is associated with poor clinical outcomes in patients with HGSC (18).

To determine whether CAF-derived MFAP5 in the tumor microenvironment can upregulate *LPP* in endothelial cells, we performed a correlative study of MFAP5 expression levels in CAFs and LPP expression levels in MECs in 96 HGSC tissue samples. We found that CAF-derived MFAP5 expression was significantly correlated with endothelial LPP expression (Figure 3A). To determine whether CAF-derived MFAP5 upregulates LPP in endothelial cells, we treated TIME and human MEC-1 (hMEC-1) cells with recombinant MFAP5 (recMFAP5) or PBS. qRT-PCR and Western blot analyses showed that cells treated with recMFAP5 had significantly higher *LPP* levels than did those treated with PBS (Figure 3, B and C).

Silencing of Mfap5 downregulates endothelial Lpp expression and reduces intratumoral microvessel densities and tumor progression in vivo. To determine the roles of *MFAP5* in regulating endothelial *LPP* expression and modulating tumor progression and angiogenesis in vivo, we first injected mice i.p. with A224 ovarian cancer cells. Two weeks after tumor cell injection, ovarian cancer–bearing mice were injected via the tail veins with chitosan nanoparticles with one of two different murine *Mfap5*-targeting siRNAs or control scrambled siRNA (Figure 3D). Using the IVIS 200 Bioluminescence and Fluorescence Imaging System (Caliper Life Sciences), we detected markedly lower luciferase activity in the *Mfap5*-targeting siRNA groups than in the control group (Figure 3, E and F). By week 6, we euthanized the mice and resected their tumors; the tumor weights in the *Mfap5*-targeting siRNA groups were significantly lower than were tumor weights in the scrambled siRNA-treated group ($P < 0.001$) (Figure 3G). Immunolocalization of murine Mfap5 and CD34 on paraffin-embedded sections of ovarian tumors from mice showed markedly lower stromal Mfap5 expression and lower CD34-positive microvessel densities in the *Mfap5*-targeting siRNA groups than in the control group, confirming that nanoparticle-delivered *Mfap5*-targeting siRNAs knocked down Mfap5 expression and reduced intratumoral microvessel densities (Figure 3H).

We further confirmed that CAF-derived Mfap5 regulates endothelial Lpp expression using a mouse model in which ovarian cancer cells were directly injected into the ovaries, and the aforementioned chitosan nanoparticle treatment schedule was used. Tumors from mice with stromal *Mfap5* silencing had markedly lower CD34-positive microvessel densities than did tumors from mice without stromal *Mfap5* silencing (Figure 3I). Immunostaining analysis revealed that the tumor tissue samples harvested from mice treated with *Mfap5*-targeting siRNAs had significantly lower endothelial Lpp expression than did those from mice treated with the scrambled siRNA, confirming that knockdown of Mfap5 downregulates endothelial Lpp expression (Figure 3J).

Fibroblast-derived MFAP5 enhances intratumoral microvessel formation. To confirm the role of fibroblast-derived MFAP5 in the regulation of endothelial *LPP* and tumor angiogenesis in vivo, we s.c. coinjected nude mice with A224 ovarian cancer cells and ovarian fibroblasts, which had been transfected with MFAP5 full-length cDNA or a mock transfectant. Compared with those from mice injected with control fibroblasts, the tumors from mice injected with MFAP5-transfected fibroblasts showed a marked increase in progression, as demonstrated by increased cancer cell bioluminescence, dry tumor weights (Supplemental Figure 4, A and B), and higher microvessel density (Supplemental Figure 4, C and D). These data suggest that fibroblast-derived MFAP5 facilitates tumor angiogenesis and increases tumor growth rates in vivo. Furthermore, immunolocalization of Lpp on tissue sections revealed that endothelial Lpp expression in tumors formed from *MFAP5*-transfected, fibroblast-injected cells was substantially

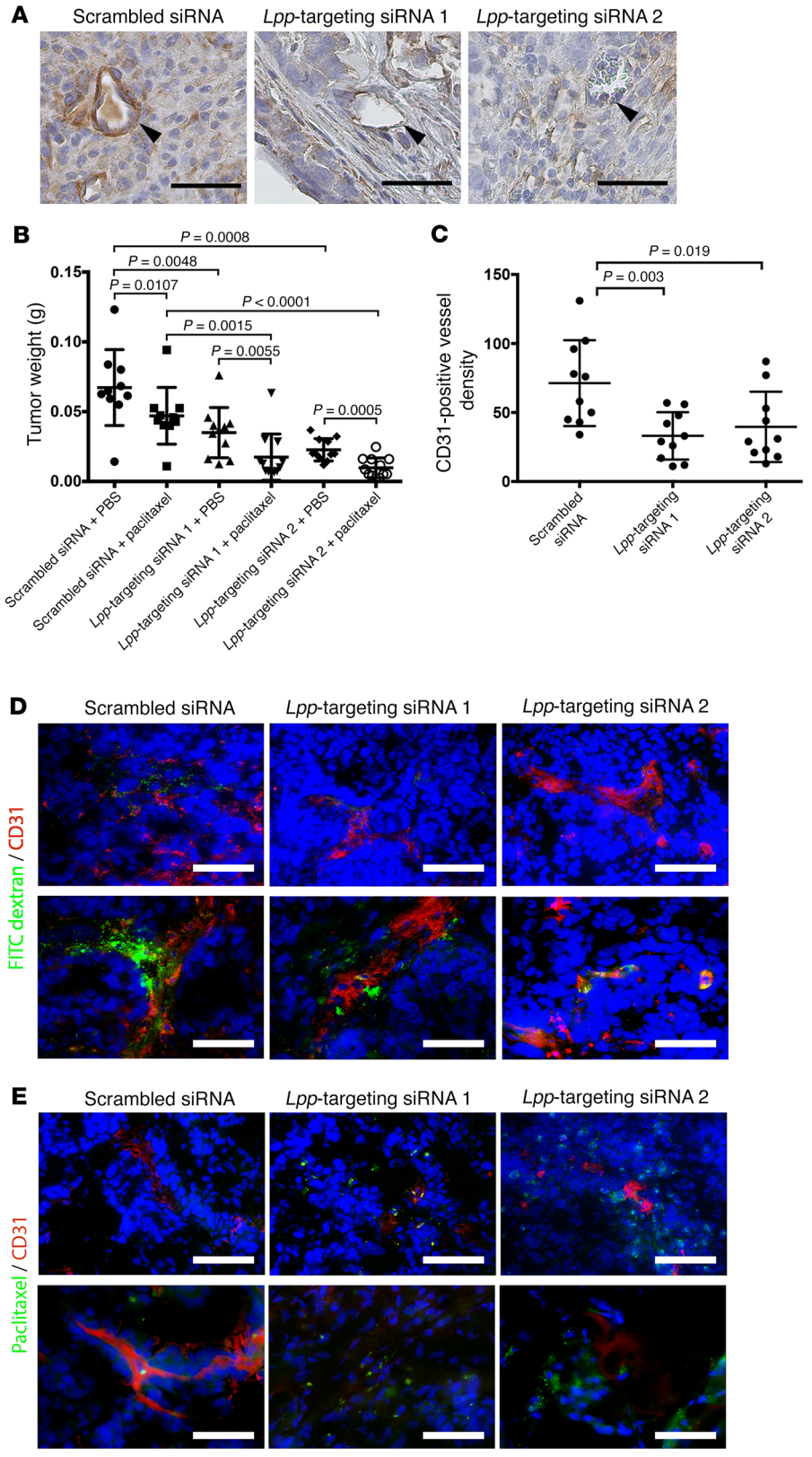

Figure 2. LPP silencing increases paclitaxel uptake and suppresses tumor growth in vivo. (**A**) Hematoxylin- counterstained micrographs showing that endothelial Lpp expression in tumor tissues collected from mice treated with *Lpp*-targeting siRNAs was markedly lower than that in tumor tissues collected from control mice treated with scrambled siRNA (arrowheads indicate tumor microvessels). Scale bars: 50 μm. (**B**) Mice treated with *Lpp*-targeting siRNA 1 or siRNA 2 had significantly smaller tumor burdens than did scrambled siRNA–treated mice ($P = 0.0048$ and $P = 0.0008$, respectively). In addition, paclitaxel-treated mice injected with Lpp-targeting siRNA 1 or Lpp-targeting siRNA 2 had significantly lower tumor weights than did scrambled siRNA–injected mice ($n = 10$/group; mean ± SD; $P = 0.0055$ and $P = 0.0005$, respectively, by Mann-Whitney *U* test). (**C**) Mice treated with *Lpp*-targeting siRNA 1 or siRNA 2 had significantly lower microvessel densities than did control group mice ($n = 10$/group; mean ± SD; $P = 0.019$ and $P = 0.003$, respectively, by Mann-Whitney *U* test). Microvessel densities were determined by immunolocalization of CD31-positive microvessels in harvested tumor nodules. (**D**) Fluorescence micrographs showing that the FITC-dextran signals in ovarian tumor tissues harvested from mice treated with *Lpp*-targeting siRNA 1 and from mice treated with *Lpp*-targeting siRNA 2 were significantly lower than those in ovarian tumor tissues from control mice, indicating reduced vessel leakiness in tumors from mice treated with *Lpp*-targeting siRNAs. Mice were injected with FITC-dextran via the tail vein 1 hour before sacrifice. Tumor vessel leakiness was evaluated by fluorescence microscopic quantification of tumor tissue FITC-dextran signals. Green: FITC-dextran; red: CD31. (**E**) Fluorescence-labeled paclitaxel signals in ovarian tumor tissues harvested from mice treated with *Lpp*-targeting siRNA 1 and from mice treated with Lpp-targeting siRNA 2 were significantly higher than those in control tumor tissues, suggesting increased drug delivery to the tumors via circulation in mice treated with *Lpp*-targeting siRNAs. Mice were injected with Oregon Green 488 fluorescence–labeled paclitaxel via the tail vein 1 hour before sacrifice. Drug delivery was evaluated by quantifying the green fluorescence signals in the tumor tissue. Green: Oregon Green 488–paclitaxel; red: CD3. (**D** and **E**) Scale bars: 100 μm (top), 50 μm (bottom).

higher than that in tumors formed from control fibroblast–injected cells, suggesting that fibroblast-derived MFAP5 upregulates endothelial *LPP* expression (Supplemental Figure 4E).

recMFAP5 upregulates endothelial LPP expression and promotes angiogenesis in vivo. To determine the extent to which MFAP5 protein promotes endothelial *LPP* expression, tumor progression, and angiogenesis in vivo, mice were implanted i.p. with Matrigel plugs reconstituted in recMFAP5 or control buffer. A histological analysis revealed that recMFAP5-containing Matrigel implants had more CD31-positive endothelial cells than did those containing PBS (Figure 4A). In addition, using the angiogenesis module of the MetaMorph imaging analysis software program (Molecular Devices) to determine the phenotype of infiltrated endothelial cells, we found that the recMFAP5-containing Matrigel implants had significantly longer total tube lengths, higher total tube areas, more segments, and more nodes than did the PBS-containing Matrigel implants (Figure 4B). To determine whether recMfap5 directly upregulates endothelial *Lpp* in vivo, we performed transcriptome profiling and qRT-PCR analyses, which showed significantly higher levels of *Lpp* mRNA in endothelial cells isolated from Matrigel plugs reconstituted in recMfap5 than in endothelial cells isolated from Matrigel plugs reconstituted in PBS (Figure 4, C and D). Upregulation of endothelial Lpp protein expression by recMfap5 in these i.p. implants was confirmed by immunostaining (Figure 4E). These data suggest that MFAP5 indeed upregulates *LPP* in MECs in vivo.

LPP mediates the effect of MFAP5 on endothelial cell motility and monolayer permeability. To determine whether *LPP* mediates the effect of *MFAP5* on endothelial cell motility, we treated hMEC-1 and TIME human MECs transfected with *LPP*-targeting siRNAs or control scrambled siRNA with recMFAP5 or control buffer. Cells treated with MFAP5 had markedly increased motility potential, which was abrogated in cells transfected with *LPP*-targeting siRNAs but not in cells transfected with scrambled siRNA (Figure 5A), suggesting that *LPP* mediated the effects of *MFAP5* on endothelial cell motility. In addition, we found that 3 times as many hMEC-1 and TIME cells invaded through porous cell culture inserts coated with Matrigel in recMFAP5-treated wells compared with that observed in control wells. Again, cells transfected with scrambled siRNA were significantly more invasive than were those transfected with *LPP*-targeting siRNAs (Figure 5B). These data suggest that LPP mediates the effect of MFAP5 on the invasive potential of these cells.

Furthermore, a tube formation assay demonstrated that hMEC-1 and TIME cells seeded on Matrigel containing recMFAP5 had a dose-dependent tubular network formation that was enhanced compared with that in cells seeded on control Matrigel (Figure 5C). Further analysis using the angiogenesis module of MetaMorph imaging analysis software revealed that the total tube lengths, total tube areas, number of segments, and number of branch points of tubes formed from hMEC-1 and TIME cells seeded onto MFAP5-containing Matrigel were significantly and dose-dependently greater than those of tubes formed from cells seeded onto control Matrigel ($P < 0.05$) (Figure 5D). In addition, the effect of recMFAP5 on tube formation was abrogated in endothelial cells transfected with *LPP*-targeting siRNAs but not in cells transfected with scrambled siRNA. These data further support the notion that *LPP* mediates the proangiogenic roles of *MFAP5* (Supplemental Figure 5, A and B).

To evaluate the effect of *MFAP5* on endothelial cell monolayer permeability in vitro, we plated hMEC-1 and TIME cells onto the E-plate of an xCELLigence system (ACEA Biosciences) to create confluent monolayer cultures and used a real-time cell analyzer to measure impedance in the presence or absence of recMFAP5. Endothelial cell monolayer cultures treated with recMFAP5 had markedly lower impedance than did those without recMFAP5 treatment, suggesting a disruption of the endothelial monolayer barrier by MFAP5 (Figure 5E). To validate this observation, we performed an in vitro permeability assay by measuring the traversal of FITC-dextran probes (molecular mass, 70,000 kDa) through hMEC-1 and TIME cell monolayers to the bottom of a Transwell in the presence or absence of recMFAP5. The amount of fluorescence-labeled dextran in the recMFAP5-containing bottom wells was larger than that in the bottom wells that did not contain recMFAP5 (Figure 5F). To determine whether *LPP* mediates the effect of *MFAP5* on endothelial cell monolayer permeability, we repeated the above experiments using endothelial cells transfected with *LPP*-targeting siRNAs or scrambled siRNA and observed that silencing *LPP* in endothelial cells abrogated the effects of MFAP5 on endothelial cell monolayer permeability (Figure 5G).

While MFAP5 mediated the motility and monolayer permeability of endothelial cells via upregulation of LPP expression, proliferation assay results showed that endothelial cell proliferation was not significantly affected by MFAP5 (Supplemental Figure 6).

LPP mediates the effect of MFAP5 on focal adhesions and stress fiber formation. Capillary endothelium permeability and endothelial cell motility are modulated by mechanical forces that are conveyed by the ECM and focal adhesion formation (19–24). To determine the mechanism by which *LPP* modulates endothelial cell motility and microvessel permeability, we used immunofluorescence microscopy to assess the colocalization of LPP and key proteins associated with focal adhesions, including paxillin, FAK, and vinculin. LPP colocalized with all 3 molecules in the focal adhesions located at the cell membrane of the endothelial cells (Figure 6A), suggesting that LPP is a key component of the focal adhesions of endothelial cells. To determine the roles of LPP in focal adhesion formation, we silenced *LPP* in TIME and hMEC-1 MECs and used vinculin/LPP staining to determine the number of focal adhesions. Cells transfected with *LPP*-targeting siRNAs had significantly fewer focal adhesions than did those transfected with control scrambled siRNA (Figure 6B and Supplemental Figure 7A), suggesting that *LPP* plays a role in focal adhesion formation. The role of *LPP* in stress fiber formation was also determined by F-actin staining. TIME cells transfected with *LPP*-targeting siRNAs had markedly less stress fiber formation than did cells transfected with scrambled siRNA (Figure 6B and Supplemental Figure 7A).

Because we found that *MFAP5* upregulates *LPP* in MECs, we determined whether *MFAP5* increased focal adhesions and stress fiber formation in MECs. We treated hMEC-1 and TIME cells with recMFAP5 or PBS and assessed the number of focal adhesions and amount of stress fiber formation. Compared with cells treated with PBS, hMEC-1 and TIME cells treated with recMFAP5 had markedly increased focal adhesions and stress fiber formation (Figure 6,

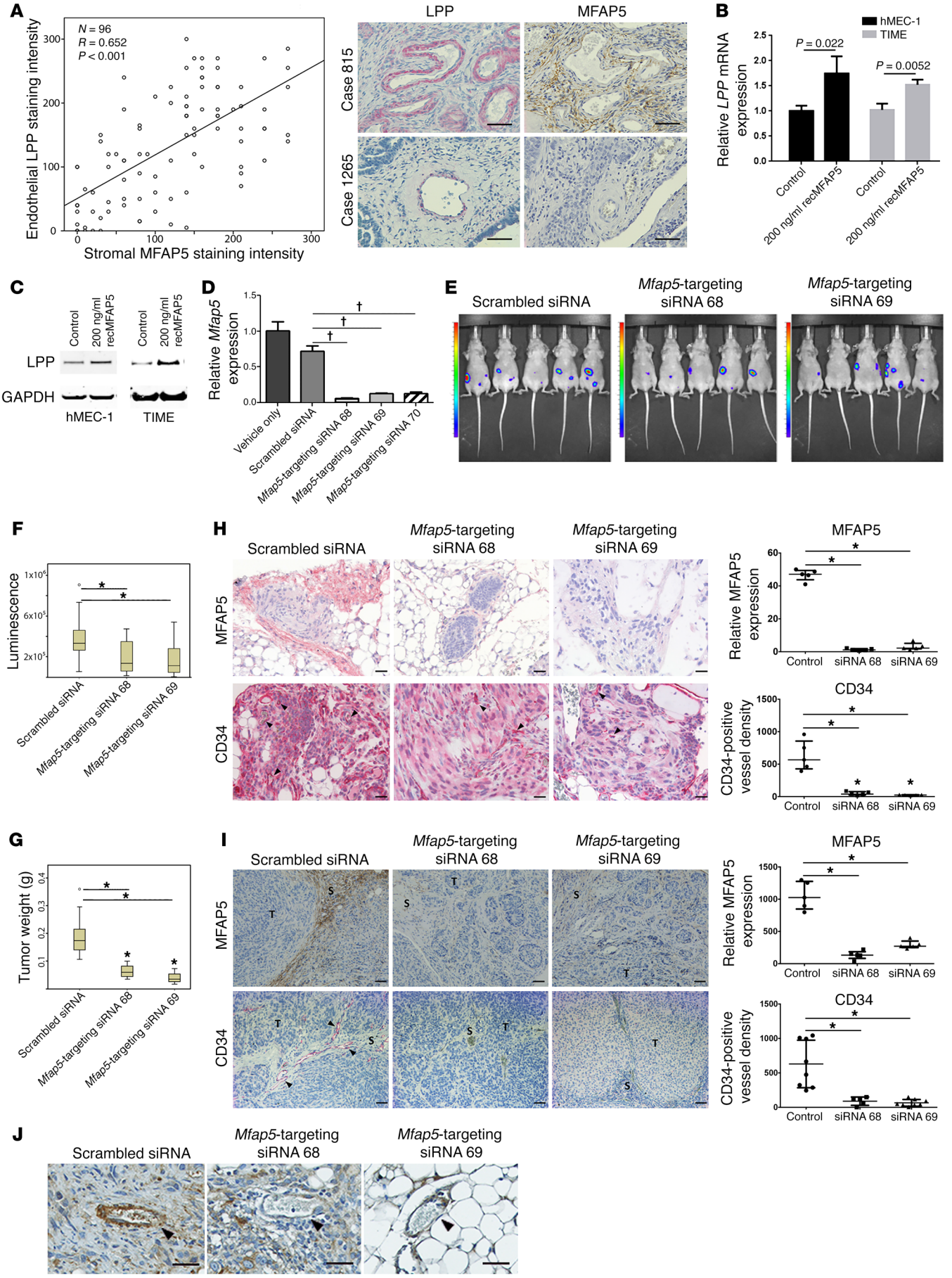
A
N = 96
R = 0.652
P < 0.001
Endothelial LPP staining intensity
Stromal MFAP5 staining intensity
LPP
MFAP5
Case 815
Case 1265
B
hMEC-1
TIME
P = 0.022
P = 0.0052
Relative LPP mRNA expression
Control
200 ng/ml recMFAP5
C
Control
200 ng/ml recMFAP5
LPP
GAPDH
hMEC-1
TIME
D
Relative Mfap5 expression
Vehicle only
Scrambled siRNA
Mfap5-targeting siRNA 68
Mfap5-targeting siRNA 69
Mfap5-targeting siRNA 70
E
Scrambled siRNA
Mfap5-targeting siRNA 68
Mfap5-targeting siRNA 69
F
Luminescence
Scrambled siRNA
Mfap5-targeting siRNA 68
Mfap5-targeting siRNA 69
H
Scrambled siRNA
Mfap5-targeting siRNA 68
Mfap5-targeting siRNA 69
MFAP5
CD34
Relative MFAP5 expression
CD34-positive vessel density
Control
siRNA 68
siRNA 69
G
Tumor weight (g)
Scrambled siRNA
Mfap5-targeting siRNA 68
Mfap5-targeting siRNA 69
I
Scrambled siRNA
Mfap5-targeting siRNA 68
Mfap5-targeting siRNA 69
MFAP5
CD34
Relative MFAP5 expression
CD34-positive vessel density
Control
siRNA 68
siRNA 69
J
Scrambled siRNA
Mfap5-targeting siRNA 68
Mfap5-targeting siRNA 69

Figure 3. CAF-derived MFAP5 modulates endothelial LPP expression and tumor vasculature. (**A**) Plot shows a significant correlation between LPP expression in endothelial cells and MFAP5 expression in CAFs (n = 96; R = 0.652, P < 0.001, by Spearman rank correlation). Hematoxylin-counterstained images of immunolocalization of MFAP5 and LPP in 2 HGSC tissue samples showing that high levels of endothelial LPP expression were associated with high levels of stromal MFAP5 (Case 815) and that low levels of endothelial LPP expression were associated with low levels of stromal MFAP5 (Case 1265). Scale bars: 50 μm. (**B**) qRT-PCR analyses show that TIME and hMEC-1 MECs treated with recMFAP5 had significantly higher levels of LPP mRNA than did PBS-treated MECs (mean ± SEM of 3 independent experiments; P values were determined by 2-tailed Student's t test). (**C**) Western blots show that TIME and hMEC-1 MECs treated with recMFAP5 had markedly increased LPP protein expression levels compared with PBS-treated MECs. (**D**) Murine fibroblasts transfected with 3 different *Mfap5*-specific siRNAs had significantly lower levels of *Mfap5* mRNA expression than did those transfected with the scrambled siRNA or the vehicle (mean ± SEM of 3 independent experiments; $^{\dagger}P$ < 0.001, by 2-tailed Student's t test). (**E**) Bioluminescence images showing markedly decreased luciferase signals in A224 ovarian tumor–bearing mice treated with chitosan nanoparticles incorporated with *Mfap5*-targeting siRNAs compared with mice injected with chitosan nanoparticles incorporated with the scrambled siRNA. Tumor growth was monitored using the IVIS 200 Bioluminescence and Fluorescence Imaging System. (**F**) Box and whisker plot showing significantly lower luminescence signal intensities in mice treated with chitosan nanoparticles incorporated with *Mfap5*-targeting siRNA 68 and *Mfap5*-targeting siRNA 69 than signals in mice injected with chitosan nanoparticles incorporated with the scrambled siRNA. Boxes represent the interquartile range of the records, and the lines across the boxes indicate the median. Whiskers indicate the highest and lowest values that were no greater than 1.5 times the interquartile range (n = 10 per group; $^{*}P$ < 0.01, by Mann-Whitney U test). (**G**) Box and whisker plot showing that the tumor weights in mice treated with *Mfap5*-targeting siRNA were significantly lower than tumor weights in mice treated with scrambled siRNA at the experimental endpoint (n = 10/group; $^{*}P$ < 0.01, by Mann-Whitney U test). (**H**) Hematoxylin-counterstained images of immunolocalization of murine Mfap5 and CD34 show that tumors from *Mfap5*-targeting siRNA– treated mice had markedly lower stromal Mfap5 expression and lower CD34-positive microvessel densities than did tumors from control mice (n = 5 per group; mean ± SD; $^{*}P$ < 0.01, by Mann-Whitney U test). Tumor cells were injected i.p. Scale bars: 50 μm. (**I**) Hematoxylin-counterstained images of immunolocalization of murine Mfap5 and CD34 show that tumors from *Mfap5*-targeting siRNA– treated mice had markedly lower stromal Mfap5 expression and lower CD34-positive microvessel densities than did tumors from control mice (n = 5 per group; mean ± SD; $^{*}P$ < 0.01, by Mann-Whitney U test). Tumor cells were delivered by intraovarian injection. Scale bars: 50 μm. S, Stroma; T, Tumor. (**J**) Hematoxylin-counterstained images of immunolocalization of Lpp show that tumors from mice treated with *Mfap5*-targeting siRNAs had significantly lower endothelial Lpp expression levels than did those treated with scrambled siRNA. Arrowheads indicate microvessels in the tumor tissue. Scale bars: 50 μm.

C and D). Immunofluorescence microscopy to assess the colocalization of LPP and F-actin revealed that MFAP5-treated cells also had markedly more stress fibers attached to upregulated *LPP* in focal adhesions on the cell membrane (Figure 6E).

To confirm that *LPP* mediates the effect of *MFAP5* on increasing stress fiber formation and focal adhesions, we transfected TIME and hMEC-1 cells with *LPP*-targeting siRNAs or scrambled siRNA and then treated the cells with recMFAP5 or PBS. Stress fiber formation and focal adhesions were determined by F-actin and vinculin LPP staining, respectively. Compared with cells treated with PBS, those treated with recMFAP5 had markedly increased stress fiber formation and focal adhesions, and these effects were abrogated in cells transfected with *LPP*-targeting siRNAs but not in cells transfected with scrambled siRNA (Figure 6F and Supplemental Figure 7B).

Taken together, our data demonstrate that *LPP* mediates the effect of *MFAP5* in the enhancement of focal adhesion and stress fiber formation, which may lead to increased endothelial cell motility and increased contractile forces within the cells, thus increasing microvessel permeability.

CAF-derived MFAP5 increases paclitaxel uptake and suppresses tumor growth in vivo. Since our data showed that CAF-derived MFAP5 upregulates LPP expression in endothelial cells and our in vitro studies suggest that *LPP* silencing promotes the delivery of paclitaxel via blood vessels to cancer cells, increasing the bioavailability of the agent to cancer cells in mice, we hereby determined the effects of *MFAP5* on paclitaxel resistance in ovarian tumor–bearing mice.

In this experiment, nude mice were s.c. coinjected with OVCA432 ovarian cancer cells with control ovarian fibroblasts or *MFAP5*-overexpressing ovarian fibroblasts. One week after the initial cancer cell and fibroblast injection, tumor-bearing mice were given weekly paclitaxel (3.5 mg/kg) injections via the tail vein for 2 weeks. One hour prior to euthanasia at the experimental endpoint, half the mice were injected with FITC-dextran via the tail vein for the evaluation of tumor vessel leakiness, and the remaining mice were injected with Oregon Green 488 green fluorescence–labeled paclitaxel via the tail vein for the evaluation of drug delivery within the tumor tissue. After euthanasia, s.c. tumor nodules were harvested and weighed. The experimental results showed that mice injected with a mixture of OVCA432 ovarian cells and MFAP5-overexpressing fibroblasts had significantly larger tumor burdens than did mice injected with a mixture of OVCA432 ovarian cancer cells and control fibroblasts on the basis of bioluminescence and tumor weights (P = 0.0138 and P < 0.0001, respectively) (Supplemental Figure 8A), suggesting that *MFAP5* confers paclitaxel resistance to OVCA432 ovarian cancer cells.

To determine whether the presence of *MFAP5* promotes tumor vessel leakiness and decreases paclitaxel delivery to ovarian cancer cells, we examined FITC-dextran and Oregon Green 488 green fluorescence–labeled paclitaxel on frozen tissue sections prepared from the harvested tumor nodules. Compared with tissues from mice injected with control fibroblasts, ovarian tumor tissues from mice injected with *MFAP5*-overexpressing fibroblasts had a significantly higher FITC-dextran signal (Supplemental Figure 8B), suggesting that MFAP5 increases vessel leakiness in the tumor tissue of these mice. The fluorescence-labeled paclitaxel signal in ovarian tumor tissues harvested from mice injected with *MFAP5*-overexpressing fibroblasts was markedly lower than that in tumor tissues from control mice (Supplemental Figure 8C), suggesting that *MFAP5* reduces the delivery of paclitaxel via blood vessels to cancer cells and subsequently decreases the bioavailability of the agent to cancer cells in these mice.

CAF-derived MFAP5 activates LPP through the calcium-dependent MFAP5/FAK/ERK/LPP signaling pathway. Our data indicated that *LPP* is a key downstream effector molecule that plays a role in modulating the effect of *MFAP5* on endothelial cell motility

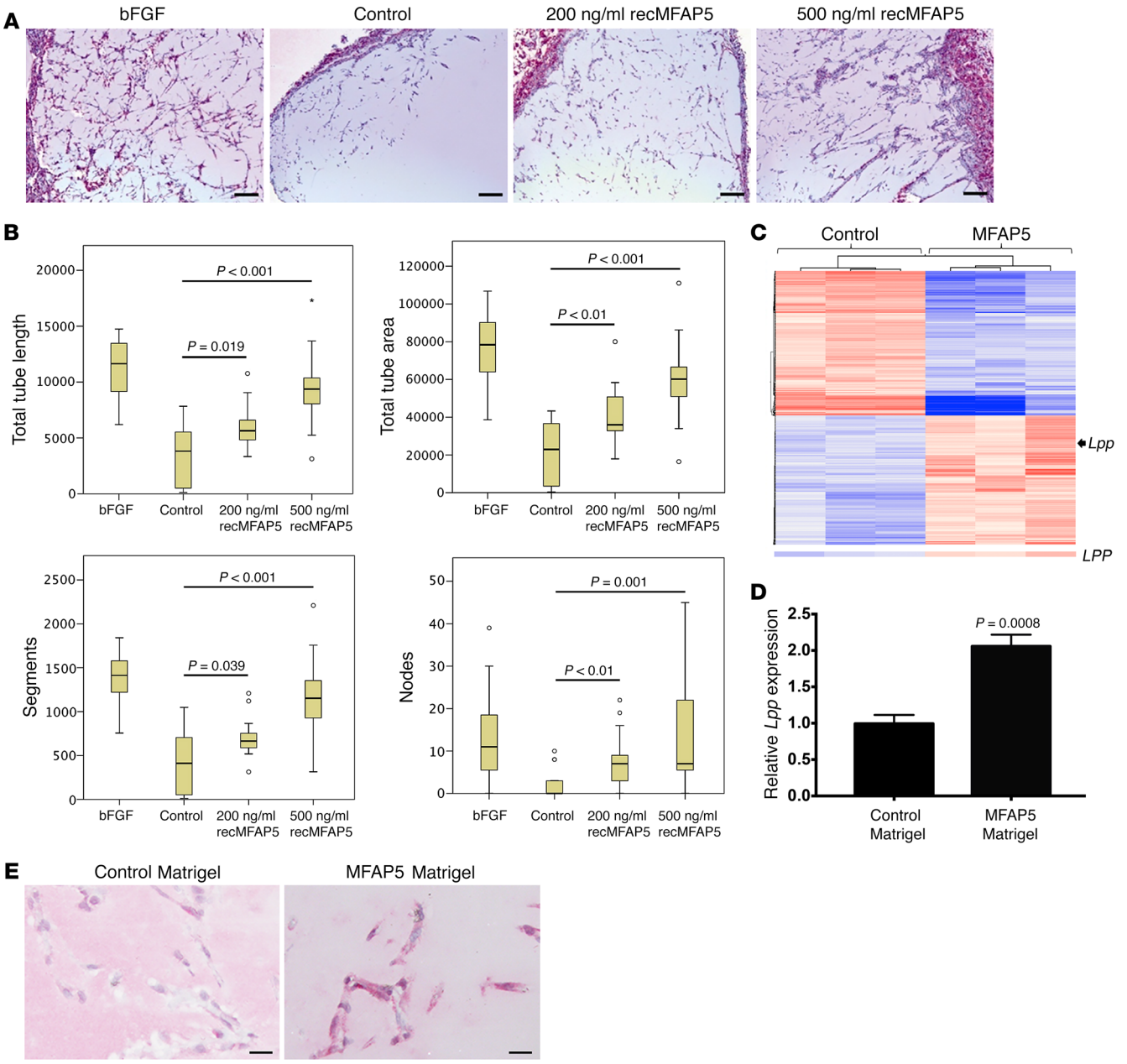

Figure 4. CAF-derived MFAP5 upregulates endothelial LPP expression and promotes angiogenesis in vivo. (**A**) Micrographs showing that recMFAP5-containing Matrigel plugs implanted i.p. into mice had significantly more CD31-positive endothelial cells than did PBS-containing Matrigel implants. Matrigel reconstituted with basic FGF (bFGF), a known proangiogenic protein, was used as a positive control. Scale bars: 100 μm. (**B**) Box and whisker plots showing the effect of recMFAP5 on total tube length, total tube area, and segment and node numbers in Matrigel plugs reconstituted with recMFAP5. The phenotypes of the endothelial cell networks in the Matrigel implants were analyzed using MetaMorph software. Compared with that reconstituted with PBS, the Matrigel reconstituted with recMFAP5 had significantly longer total tube lengths, larger total tube areas, more segments, and more nodes. The boxes in the box plot represent the interquartile range, and the lines across the boxes indicate the median. The whiskers indicate the highest and lowest values that were no greater than 1.5 times the interquartile range (n = 10/group; P values were determined by Mann-Whitney U test). (**C**) Heatmap showing differentially expressed genes that were up- or downregulated in endothelial cells isolated from recMFAP5-containing Matrigel implants compared with cells from PBS-containing Matrigel implants in mice. Transcriptome profiling of endothelial cells isolated from Matrigel implants revealed that 394 genes were expressed at significantly higher levels and 449 genes were expressed at significantly lower levels in recMFAP5-containing Matrigel implants compared with cells from PBS-containing Matrigel implants ($P < 0.05$, by moderated t test and Benjamini-Hochberg multiple testing correction). Expression of *Lpp* was increased by 2-fold in endothelial cells isolated from recMFAP5-containing Matrigel implants compared with cells from PBS-containing Matrigel implants. (**D**) qRT-PCR analyses showing that endothelial cells isolated from recMFAP5-containing Matrigel implants had significantly higher levels of *Lpp* mRNA than did PBS-containing Matrigel implants (mean ± SEM of 3 independent experiments; 2-tailed Student's t test). (**E**) Hematoxylin-counterstained micrographs showing that endothelial cells from recMFAP5-containing Matrigel implants had markedly higher Lpp protein levels than did cells from PBS-containing Matrigel implants. Scale bars: 10 μm.

and permeability. Previous studies showed that $\alpha_v\beta_3$ integrin is a major receptor for MFAP5 and that *MFAP5* plays a role in $\alpha_v\beta_3$ integrin–mediated angiogenesis (25). In addition, Ca^{2+} mobilization is involved in integrin signaling and cell migration (26–28). We therefore hypothesized that the binding of MFAP5 to $\alpha_v\beta_3$ integrin activates calcium-dependent signaling pathways that transcriptionally upregulate LPP expression and subsequently increase the motility and permeability of endothelial cells.

To test these hypotheses, we first determined whether the effect of *MFAP5* on *LPP* expression in endothelial cells is Ca^{2+} dependent. The stimulatory effect of *MFAP5* on endothelial cell motility (Figure 7A) and stress fiber formation (Figure 7B) was abrogated in cells preloaded with the cell-permeant calcium chelator BAPTA/AM, suggesting that calcium signaling is involved in the modulation of *MFAP5* function. Moreover, using the calcium dye Fluo-4 AM and confocal fluorescence microscopy, we found that exogenous recMFAP5 mobilized intracellular Ca^{2+} in hMEC-1 cells (Figure 7C). recMFAP5-induced calcium mobilization was attenuated in cells treated with the inositol 1,4,5-triphosphate receptor inhibitor xestospongin C but not the ryanodine receptor blocker (Figure 7, D and E), suggesting that MFAP5 induces calcium release via the inositol 1,4,5-triphosphate receptor instead of the ryanodine receptor. Furthermore, we also detected store-operated calcium entry into hMEC-1 cells (Figure 7F), which might also contribute to MFAP5-induced calcium mobilization after emptying of inositol 1,4,5-triphosphate–sensitive intracellular calcium stores.

Next, we focused on intermediate signaling molecules that are implicated in the mediation of cell motility and calcium signaling. Compared with control cells, MECs treated with recMFAP5 had higher expression of phosphorylated FAK (p-FAK) (Y861), p–PLC-γ1 (Y783), p-PKCθ (T538), p-ERK1/2 (T202/Y204), phosphorylated myosin regulatory light chain 2 (p-MLC2) (T18/S19), phosphorylated cyclic AMP–responsive element-binding protein (p-CREB) (S133), c-Jun, and p–c-Jun (S73), which may have led to the upregulation of *LPP* expression and thus increased cell motility and permeability (Figure 7G).

Because our data demonstrated that MFAP5-induced microvascular endothelial cell motility was suppressed in cells that had been pretreated with an anti–$\alpha_v\beta_3$ integrin antibody (Figure 7H) and that MFAP5-upregulated p-FAK (Y861) expression was suppressed in cells that had been pretreated with BAPTA-AM (1,2-bis-[2-aminophenoxy]-ethane-*N*,*N*,*N′*,*N′*-tetraacetic acid, tetraacetoxymethyl ester) (Supplemental Figure 9A and Supplemental Figure 10A), we hypothesized that MFAP5-mediated responses in endothelial cells require the binding of MFAP5 to $\alpha_v\beta_3$ integrin, which leads to the activation of FAK. Activated FAK, in turn, activates PKCθ, which can regulate Ca^{2+} influx (29). Ca^{2+} mobilization activates ERK1/2 and leads to the phosphorylation of MLC2 and activation of CREB. The translocation of CREB to the nucleus and the binding of activated CREB to the cAMP response element of c-Jun may transcriptionally upregulate the expression of *LPP*, which contains multiple AP1-binding sites in its promoter sequence. The potential *MFAP5*-mediated signaling pathways are illustrated in Supplemental Figure 11.

To determine whether the binding of MFAP5 to $\alpha_v\beta_3$ integrin and the formation of the FAK-$\alpha_v\beta_3$ complex mediates MFAP5-induced FAK and PLC-γ1 phosphorylation, we pretreated hMEC-1 and TIME cells with an anti–$\alpha_v\beta_3$ integrin antibody (LM609), an anti-α_5 antibody, or control IgG and then treated them with recMFAP5. The effect of recMFAP5 on FAK and PLC-γ1 phosphorylation was abrogated in cells pretreated with the anti–$\alpha_v\beta_3$ integrin antibody but not the anti-α_5 antibody or control IgG (Supplemental Figure 9, B and C, and Supplemental Figure 10, B and C).

Next, we determined whether FAK phosphorylation mediates the MFAP5-induced phosphorylation of PKCθ in MECs. Western blot analysis of PKCθ in hMEC-1 and TIME cells treated with MFAP5 in the presence or absence of the FAK inhibitor PF573228 (Sigma-Aldrich) revealed that p-PKCθ expression was increased only in the absence of the FAK inhibitor (Supplemental Figure 9D and Supplemental Figure 10D).

Because previous studies demonstrated that PLC-γ1 phosphorylation can be stimulated not only by $\alpha_v\beta_3$ engagement alone (30) but also by the formation of a FAK-$\alpha_v\beta_3$ complex (31), we determined whether PLC-γ1 phosphorylation is FAK dependent. The MFAP5-induced phosphorylation of PLC-γ1 (Y783) was attenuated in hMEC-1 and TIME cells that had been pretreated with a FAK inhibitor (Supplemental Figure 9E and Supplemental Figure 10E), which suggests that MFAP5-induced PLC-γ1 (Y783) phosphorylation is FAK dependent. The MFAP5-induced phosphorylation of PKCθ was also attenuated in hMEC-1 and TIME cells that had been treated with a PLC inhibitor (U73122; sc-3574; Santa Cruz Biotechnology) (Supplemental Figure 9F and Supplemental Figure 10F), which suggests that PLC-γ1 phosphorylation regulates PKCθ activation. However, as described in a report of MFAP5-stimulated signaling in ovarian cancer cells (18), the upregulation of p–PLC-γ1 expression was abolished in cells treated with a PKCθ inhibitor, indicating that PKCθ phosphorylation and PLC-γ1 phosphorylation are interdependent (Supplemental Figure 9G and Supplemental Figure 10G).

To determine whether the ERK1/2 and CREB activation induced by MFAP5 via PKCθ and PLC-γ1 is Ca^{2+} dependent and mediated by the activation of an $\alpha_v\beta_3$ integrin/FAK/PKCθ pathway, we treated hMEC-1 and TIME cells with MFAP5 in the presence or absence of BAPTA-AM and a PKCθ pseudosubstrate inhibitor. Western blot analysis revealed that the phosphorylation of PKCθ, PLC-γ1, ERK1/2, and CREB after recMFAP5-based treatment was attenuated in BAPTA-AM–loaded cells (Supplemental Figure 9, H–K and Supplemental Figure 10, H–K). These data suggest that MFAP5-induced activation of both ERK and CREB is calcium dependent. In addition, ERK1/2 phosphorylation was abrogated in cells treated with the PKCθ pseudosubstrate inhibitor (Supplemental Figure 9L and Supplemental Figure 10L), which suggests that MFAP5-induced ERK1/2 activation depends on the $\alpha_v\beta_3$ integrin/FAK/PKCθ pathway.

Previous studies reported that MLC2 and CREB activation depends on ERK (32, 33); therefore, we determined whether calcium-dependent ERK1/2 phosphorylation mediates the activation of MLC2 and CREB. The recMFAP5-stimulated phosphorylation of MLC2 and CREB was attenuated in hMEC-1 and TIME cells treated with an ERK1/2 inhibitor (FR180204; Merck) (Supplemental Figure 9, M and N, and Supplemental Figure 10, M and N), demonstrating that MFAP5 induces MLC2 and CREB activation via ERK1/2.

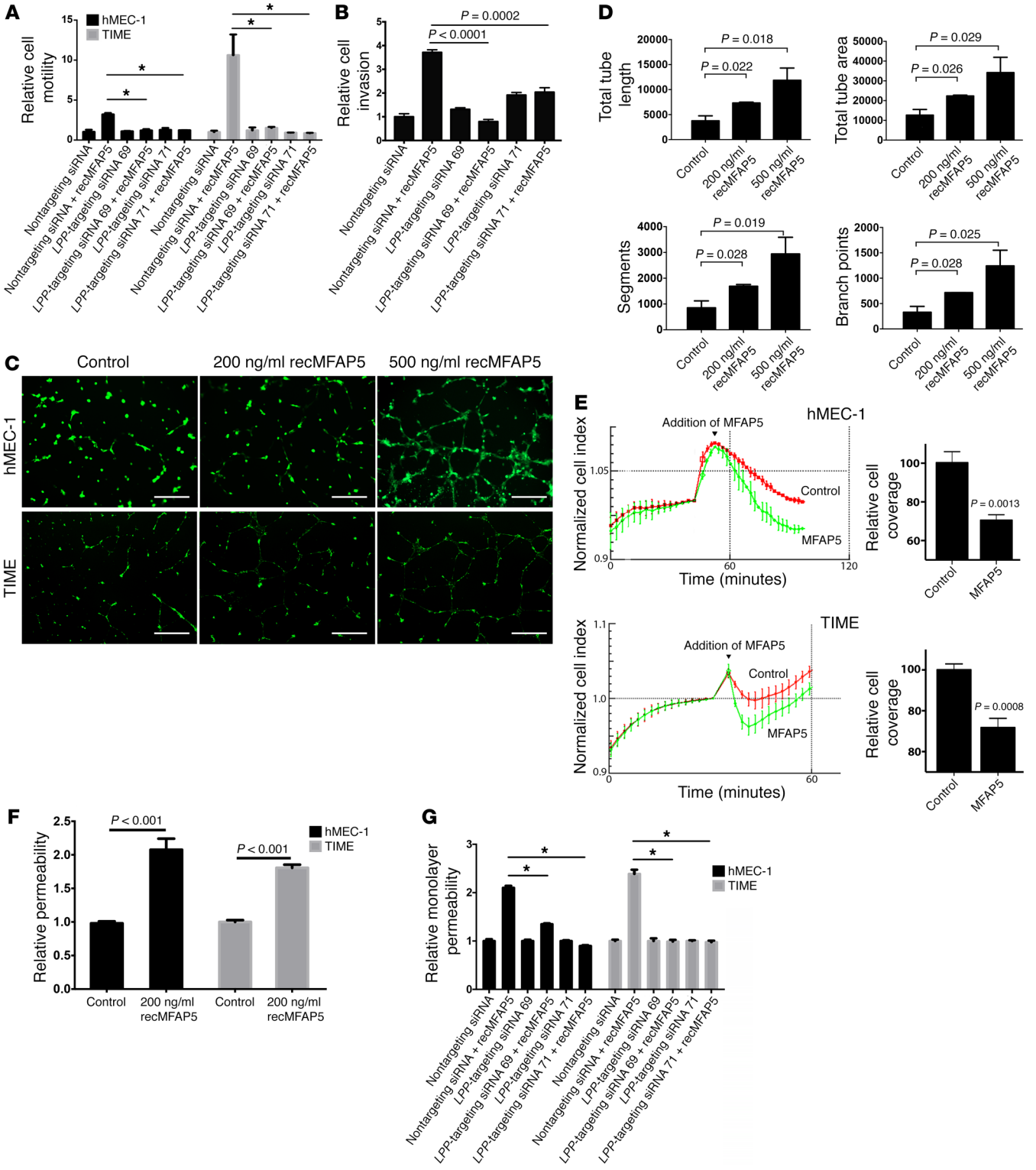
A
Relative cell motility
hMEC-1
TIME
Nontargeting siRNA
Nontargeting siRNA + recMFAP5
LPP-targeting siRNA 69
LPP-targeting siRNA 69 + recMFAP5
LPP-targeting siRNA 71
LPP-targeting siRNA 71 + recMFAP5
B
Relative cell invasion
P = 0.0002
P < 0.0001
C
Control
200 ng/ml recMFAP5
500 ng/ml recMFAP5
hMEC-1
TIME
D
Total tube length
P = 0.018
P = 0.022
Total tube area
P = 0.029
P = 0.026
Segments
P = 0.019
P = 0.028
Branch points
P = 0.025
P = 0.028
Control
200 ng/ml recMFAP5
500 ng/ml recMFAP5
E
hMEC-1
Addition of MFAP5
Normalized cell index
Control
MFAP5
Time (minutes)
Relative cell coverage
P = 0.0013
TIME
P = 0.0008
F
Relative permeability
P < 0.001
P < 0.001
hMEC-1
TIME
G
Relative monolayer permeability

Figure 5. LPP mediates the effect of MFAP5 on endothelial cell motility and monolayer permeability. (**A**) hMEC-1 and TIME endothelial cells treated with MFAP5 had markedly increased motility potential compared with control cells. This increase in motility induction was abrogated in cells transfected with *LPP*-targeting siRNA but not in cells transfected with control scrambled siRNA, which suggests that *LPP* mediates the effect of *MFAP5* on endothelial cell motility (mean ± SEM of 3 independent experiments; $^*P < 0.01$, by 2-tailed Student's *t* test). (**B**) A significantly greater number of hMEC-1 and TIME cells invaded through porous Matrigel-coated cell culture inserts in the presence of recMFAP5 than in the absence of recMFAP5. The effect of MFAP5 on promoting invasive potential was abrogated in endothelial cells transfected with *LPP*-targeting siRNAs (mean ± SEM of 3 independent experiments; *P* values were determined by 2-tailed Student's *t* test). (**C**) Micrographs show that recMFAP5 enhanced the tubular network formation of hMEC-1 and TIME cells seeded on Matrigel in a dose-dependent manner. Scale bars: 50 μm. (**D**) Image analyses showed dose-dependent increases in tube length, tube area, number of segments, and number of branch points for tubes formed from hMEC-1 and TIME cells seeded onto MFAP5-containing Matrigel compared with those formed from cells seeded onto control Matrigel (mean ± SEM of 3 independent experiments; *P* values were determined by 2-tailed Student's *t* test). (**E**) Monolayer permeability analyses using the xCELLigence system show that MFAP5-treated, confluent endothelial cell monolayer hMEC-1 and TIME cultures had a marked decrease in impedance compared with PBS-treated cells (mean ± SEM of 4 independent experiments). (**F**) Effect of MFAP5 on the permeability of endothelial cell monolayers. hMEC-1 and TIME monolayers treated with recMFAP5 had a significantly greater amount of fluorescence-labeled dextran in the bottom wells of Transwells than did those treated with PBS (mean ± SEM of 3 independent experiments; *P* values were determined by 2-tailed Student's *t* test). (**G**) Effect of *LPP* silencing on MFAP5-enhanced endothelial cell permeability. hMEC-1 and TIME monolayers treated with recMFAP5 had a significantly greater amount of fluorescence-labeled dextran in the bottom wells of Transwells than did those treated with PBS, and the effect was abrogated when hMEC-1 and TIME were transfected with *LPP*-targeting siRNA (mean ± SEM of 3 independent experiments; $^*P < 0.01$, by 2-tailed Student's *t* test).

Furthermore, our data demonstrated that c-Jun, which contains a cAMP response element in its promoter, upregulated expression in MFAP5-treated hMEC-1 and TIME cells. Promoter analysis revealed that the *LPP* promoter consists of multiple potential AP1-binding sites (Supplemental Figure 3), suggesting that the transcriptional upregulation of LPP expression is controlled by CREB-mediated c-Jun expression. To confirm this, we evaluated the effects of a CREB-binding protein–CREB (CBP-CREB) interaction inhibitor and the c-Jun inhibitor SP600125 on MFAP5-treated cells. The CBP-CREB interaction inhibitor attenuated the upregulation of both total c-Jun and p–c-Jun expression, whereas the c-Jun inhibitor SP600125 abrogated the upregulation of LPP expression (Supplemental Figure 9, O and P, and Supplemental Figure 10, O, and P). These data confirm that the MFAP5-induced increase in LPP expression is calcium dependent and is mediated by the upregulation of c-Jun expression by CREB activation.

After finding that *MFAP5* can activate the FAK/ERK/CREB signaling network to upregulate LPP expression, we determined whether *LPP* can modulate the effect of *MFAP5* on downstream signaling network activation via a positive feedback loop, as LPP can be recruited to focal adhesions in MDCK epithelial cells and interacts with α-actinin in the focal adhesion complex (13, 14, 34). Western blot analysis of FAK phosphorylation in recMFAP5-treated hMEC-1 and TIME cells transfected with *LPP*-targeting siRNAs or control scrambled siRNA revealed that *LPP*-targeting siRNA successfully abrogated MFAP5-induced FAK phosphorylation (Supplemental Figure 9Q and Supplemental Figure 10Q). In addition, knockdown of *LPP* expression attenuated an MFAP5-stimulated increase in focal adhesion formation (Figure 6, C and D). These findings suggest that focal adhesion targeting by *LPP* plays an essential role in focal adhesion complex formation and downstream signaling molecule activation, both of which mediate the effect of MFAP5 on endothelial cell motility and permeability.

Discussion

The present study demonstrates, for the first time to our knowledge, that a CAF-derived mediator elevates *LPP* expression in cancer-associated MECs in the tumor microenvironment and that *LPP*, a prognostic marker associated with poor survival rates in HGSC patients, confers paclitaxel resistance by increasing the motility and monolayer permeability of endothelial cells. Collectively, our data show, for the first time to our knowledge, that *LPP* can increase the motility of MECs and promote tumor progression. In addition, we believe our findings provide important information on the roles of CAFs in the modulation of tumor angiogenesis and chemoresistance.

MECs in tumor vessels are known to form abnormal monolayers, and they do not have a normal barrier function (35). These cells are disorganized and irregularly shaped. They also have loose interconnections and focal intercellular openings, which are probably responsible for increased vessel leakiness. We found that increased *LPP* expression facilitated the formation of focal adhesion complexes, increased cell traction force in endothelial cells, and increased leakiness in endothelial cell monolayers, suggesting that *LPP* plays an important role in the formation of disorganized microvessels within the tumor tissue. The increased focal adhesion, stress fiber formation, and traction force in cells enabled the establishment of contractile forces that pull apart the interendothelial cell junctions, thus increasing permeability.

In the present study, we showed that LPP expression modulates tumor vessel integrity. Blood vessel leakiness not only plays a role in angiogenesis, tumor growth, and metastasis but also affects drug delivery and drug resistance. Despite a severely defective barrier function and increase in diameter, tumor vessels do not facilitate drug delivery, because their high interstitial pressure limits the extravasation of fluid and macromolecules (36, 37). Our in vivo data show that *LPP* silencing significantly increased paclitaxel delivery to the tumor tissue in mice, indicating that *LPP* in MECs plays an important role in microvessel leakiness and paclitaxel delivery to tumor cells. Our data also suggest that targeting *LPP* normalizes tumor blood vessels, thereby facilitating drug delivery to tumor tissue and increasing drug efficacy.

Both cancer cells and stromal cells produce VEGF glycoproteins and proangiogenic factors, including FGFs and PDGFs. These relatively cell-type–nonspecific factors are important regulators of tumor angiogenesis, but the crucial roles of stromal-specific proangiogenic factors in tumor progression remain unclear. Antiangiogenic agents have been used to suppress uncontrolled tumor vessel formation and therefore normalize

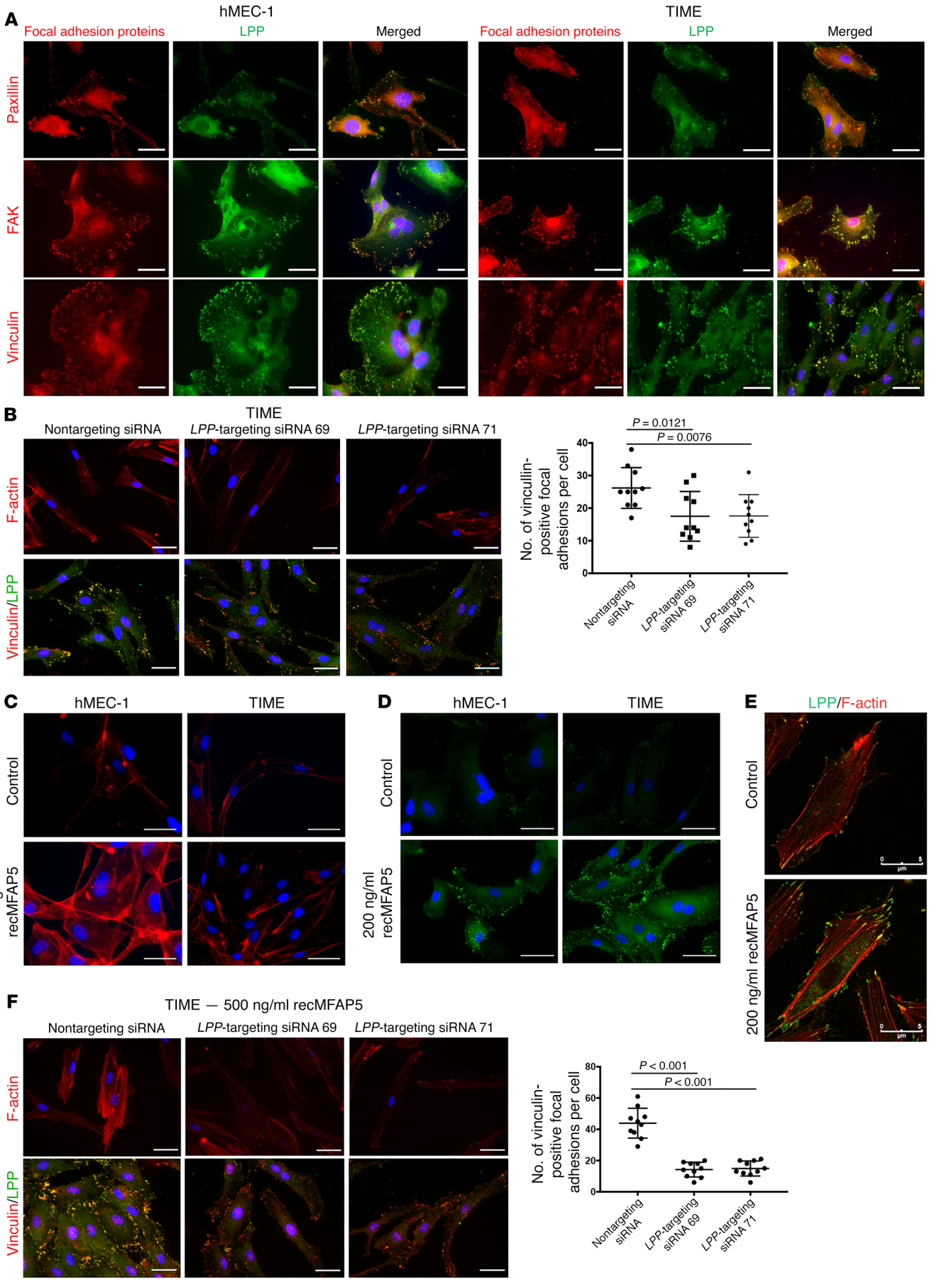
A
hMEC-1
TIME
Focal adhesion proteins
LPP
Merged
Paxillin
FAK
Vinculin
B
TIME
Nontargeting siRNA
LPP-targeting siRNA 69
LPP-targeting siRNA 71
F-actin
Vinculin/LPP
P = 0.0121
P = 0.0076
No. of vinculin-positive focal adhesions per cell
C
hMEC-1
TIME
Control
200 ng/ml recMFAP5
D
E
LPP/F-actin
F
TIME — 500 ng/ml recMFAP5
P < 0.001
P < 0.001

Figure 6. LPP mediates the effect of MFAP5 on focal adhesions and stress fiber formation. (**A**) Immunofluorescence micrographs showing that LPP colocalized with key focal adhesion proteins including paxillin, FAK, and vinculin in the focal adhesions located at the cell membrane of the 2 MEC lines hMEC-1 and TIME, suggesting that LPP is a key component of the focal adhesions of endothelial cells. Red: focal adhesion proteins; green: LPP; blue: nuclei. (**B**) Immunofluorescence micrographs showing that TIME MECs transfected with *LPP*-targeting siRNA had fewer F-actin stress fibers and focal adhesions than did cells transfected with control scrambled siRNA, suggesting that *LPP* plays important roles in stress fiber and focal adhesion formation. Dot plot summarizes the data (mean ± SD; n = 10/treatment group; P values were determined by 2-tailed Student's t test). Red: F-actin/vinculin; green: LPP; blue: nuclei. (**C**) Immunofluorescence micrographs showing that hMEC-1 and TIME MECs treated with 200 ng/ml recMFAP5 had more F-actin stress fibers and focal adhesions than did cells treated with PBS, suggesting that *MFAP5* could increase stress fiber formation in endothelial cells. Red: F-actin; blue: nuclei. (**D**) Immunofluorescence micrographs showing that hMEC-1 and TIME MECs treated with 200 ng/ml recMFAP5 had more focal adhesions than did cells treated with PBS, suggesting that *MFAP5* could increase focal adhesions in endothelial cells. Green: vinculin; blue: nuclei. (**E**) Immunofluorescence micrographs showing that recMFAP5-treated cells had markedly more stress fibers (red) attached to upregulated LPP (green) in focal adhesions on the cell membrane than did control cells. (**F**) Immunofluorescence micrographs showing that MFAP5-induced stress fiber formation and that focal adhesions were abrogated in TIME cells transfected with *LPP*-targeting siRNAs but not with the control scrambled siRNA, suggesting that *LPP* mediates the effect of *MFAP5* in increasing stress fiber formation and focal adhesions. Red: F-actin/vinculin; green: LPP; blue: nuclei. Data are summarized in the dot plot (mean ± SD of 10 independent experiments; P values were determined by 2-tailed Student's t test). Scale bars: 5 μm (**A**–**F**).

the vessel system for improved drug delivery (38–41). However, several clinical trials in cancer patients have demonstrated that agents targeting VEGF family members convey a progression-free survival advantage but rarely an overall survival advantage, possibly because other potent proangiogenic factors and their downstream effector molecules are present in the tumor microenvironment and endothelial cells, respectively, leading to insufficient suppression of tumor angiogenesis (1, 2, 42).

In the present study, we demonstrated for the first time to our knowledge that *MFAP5*, a novel CAF-derived proangiogenic marker (18), induced endothelial cell permeability and leakiness by upregulating *LPP*. We also showed that MFAP5 bound to $\alpha_v\beta_3$ integrin in MECs and thus activated a calcium-dependent FAK/ERK/MLC2/CREB signaling network to upregulate *LPP*. In addition, we demonstrated that *LPP* silencing significantly decreased *MFAP5*-activated FAK phosphorylation in endothelial cells, indicating that *LPP* in the focal adhesion complex not only facilitates the formation of stress fibers but also plays a role in activating the *MFAP5* downstream signaling network. Together, these networks of CAF–endothelial cell crosstalk may decrease the effectiveness of current antiangiogenic agents that target VEGF family members.

Our studies focused on the use of NOFs and CAFs derived from the ovarian site, since the ovary is the preferred site for ovarian cancer development. Cancer cells, derived either from the tubal epithelium or from the ovarian surface epithelium, interact with local ovarian fibroblasts or fibroblasts recruited to the ovarian site during tumor development. As the disease progresses, tumor spreads to the omentum, which is the preferred metastatic disease site for ovarian cancer cells (43). Further study of the interaction between omental CAFs and metastatic ovarian cancer cells could provide additional insights into the roles of CAFs in ovarian cancer progression.

In conclusion, we characterized the roles of *LPP* in ovarian cancer angiogenesis and delineated the underlying mechanism by which CAF-derived MFAP5 modulates *LPP* expression in endothelial cells. In addition, our data highlight the importance of the activation of CAF–endothelial cell crosstalk signaling in modulating chemoresistance in patients with ovarian cancer. More important, we demonstrated the feasibility and improved the efficacy of using *LPP*-targeting siRNA in combination with cytotoxic drugs as a treatment for ovarian cancer. Our findings support the idea that therapies targeting both CAFs and endothelial cells in the ovarian tumor microenvironment may synergize with other cancer cell–targeting regimens to increase treatment efficacy.

Methods

Cell lines and culture conditions. hMEC-1 cells were cultured in MCDB131 medium supplemented with 10% FBS, 10 mM L-glutamine, 10 ng/ml EGF, and 1 μg/ml hydrocortisone. TIME cells were cultured in endothelial cell growth medium-2 (Lonza). Both endothelial cell lines were obtained from the ATCC. The ovarian adenocarcinoma cell lines A224 (gift of Michael Birrer's laboratory, University of Alabama, Tuscaloosa, Alabama, USA) and OVCA432 (gift of Robert Bast's laboratory, The University of Texas MD Anderson Cancer Center) were maintained in RPMI 1640 medium supplemented with 10% FBS and 2 mM glutamine. Human fibroblast cultures were maintained in 1:1 MCDB105/199 medium supplemented with 10% FBS and 1 ng/ml EGF.

In vivo silencing of endothelial Lpp. To evaluate the effects of endothelial *LPP* expression on ovarian tumor progression in vivo, we i.p. injected 2×10^6 luciferase-labeled OVCA432 cells into 6-week-old female nude mice (Envigo). OVCA432 ovarian tumor–bearing mice were given twice-weekly tail-vein injections of chitosan nanoparticles with 5 μg control scrambled siRNA, murine *Lpp*–targeting siRNA 1, or murine *Lpp*–targeting siRNA 2 and weekly i.p. injections of either sterile PBS or paclitaxel (3.5 mg/kg) for 6 weeks. For each experiment group, half the animals were given 100 μl of 10 mg/ml FITC-dextran (Sigma-Aldrich) via the tail vein before evaluation of intratumoral blood vessel leakiness; the remaining animals received Oregon Green 488–conjugated paclitaxel (1 mg/kg; Life Technologies, Thermo Fisher Scientific) via i.v. injection 1 hour before they were evaluated for paclitaxel biodistribution. All mice in all treatment groups were euthanized at the experimental endpoint. Intraperitoneal tumor nodules were harvested, weighed, and fixed for histological analysis. In addition to formalin tissue sections, 6-μm frozen tissue sections were prepared from tumors harvested using a CM1850 cryostat (Leica Microsystems) to evaluate the effect of *LPP* silencing on intratumoral microvessels and the bioavailability of paclitaxel by fluorescence microscopy.

In vivo silencing of stromal Mfap5. To determine the roles of *MFAP5* in regulating endothelial *LPP* expression and modulating tumor progression and angiogenesis in vivo, we injected 2×10^6 A224 ovarian cancer cells i.p. into 6-week-old female nude mice (Envigo). Two weeks after tumor cell injection, ovarian cancer–bearing mice were

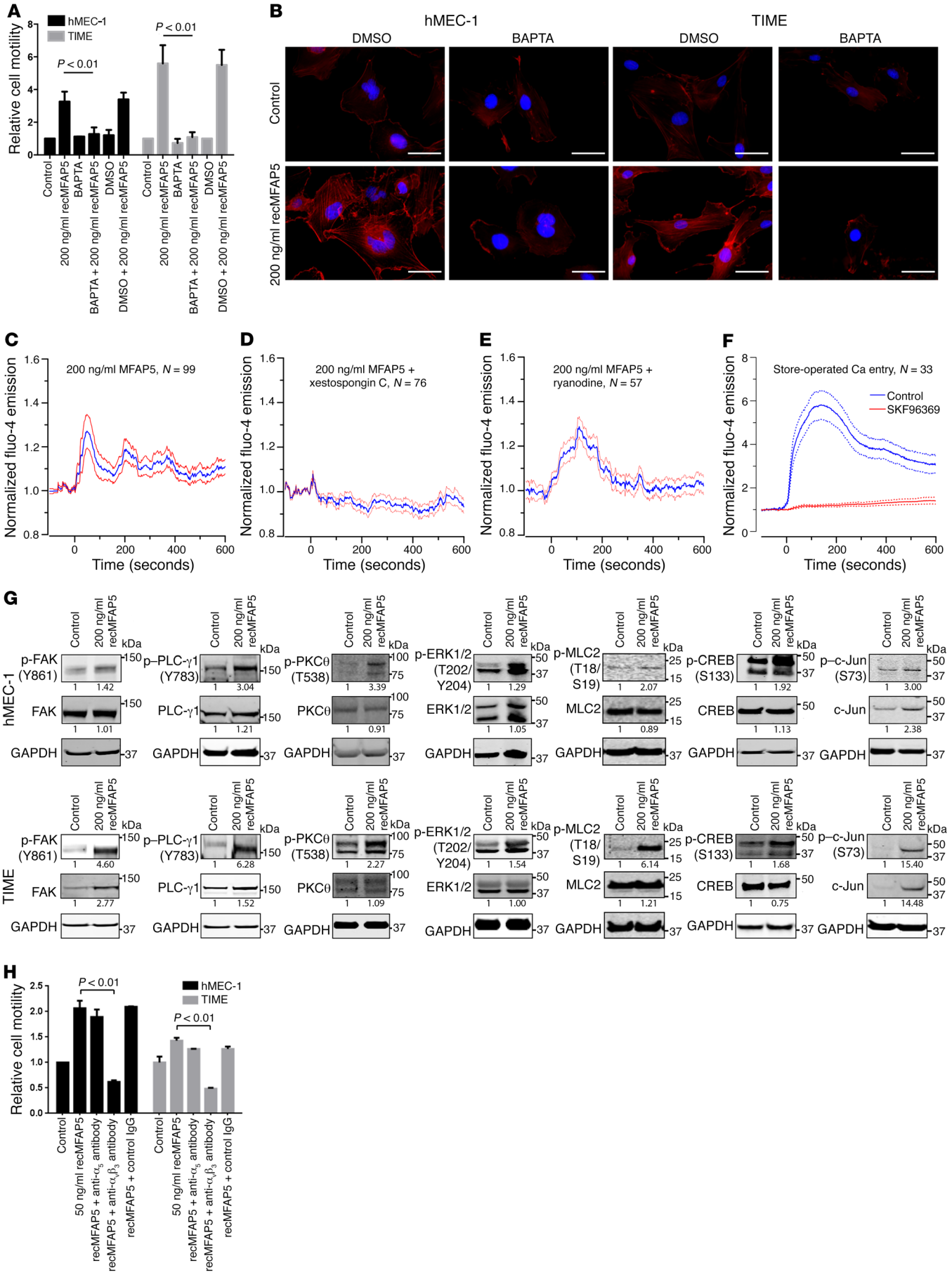
A
hMEC-1
TIME
Relative cell motility
P < 0.01
P < 0.01
Control
200 ng/ml recMFAP5
BAPTA
BAPTA + 200 ng/ml recMFAP5
DMSO
DMSO + 200 ng/ml recMFAP5
B
hMEC-1
TIME
DMSO
BAPTA
Control
200 ng/ml recMFAP5
C
200 ng/ml MFAP5, N = 99
D
200 ng/ml MFAP5 + xestospongin C, N = 76
E
200 ng/ml MFAP5 + ryanodine, N = 57
F
Store-operated Ca entry, N = 33
Control
SKF96369
Normalized fluo-4 emission
Time (seconds)
G
hMEC-1
TIME
p-FAK (Y861)
FAK
p-PLC-γ1 (Y783)
PLC-γ1
p-PKCθ (T538)
PKCθ
p-ERK1/2 (T202/Y204)
ERK1/2
p-MLC2 (T18/S19)
MLC2
p-CREB (S133)
CREB
p–c-Jun (S73)
c-Jun
GAPDH
kDa
H
Relative cell motility
P < 0.01
P < 0.01
hMEC-1
TIME
50 ng/ml recMFAP5
recMFAP5 + anti-α5 antibody
recMFAP5 + anti-αvβ3 antibody
recMFAP5 + control IgG

Figure 7. CAF-derived MFAP5 activates LPP through the calcium-dependent MFAP5/FAK/ERK/LPP signaling pathway. (**A**) hMEC-1 and TIME MECs treated with recMFAP5 had significantly higher motility rates than did MECs treated with the control buffer, and the stimulatory effect of MFAP5 on cell motility was abrogated in cells preloaded with the cell-permeant calcium chelator BAPTA-AM (mean ± SEM of 3 independent experiments; $P < 0.01$, by 2-tailed Student's *t* test). (**B**) Fluorescence micrographs show that MFAP5-induced stress fiber formation was abrogated in MECs that had been preloaded with BAPTA-AM, suggesting that calcium signaling is involved in modulating MFAP5 function. Red: F-actin; blue: nuclei. Scale bars: 5 μm. (**C**–**E**) Mean normalized time courses of calcium mobilization induced by treating hMEC-1 cells with recMFAP5 in the absence and presence of calcium channel blockers. Calcium influx was monitored with confocal fluorescence microscopy. recMFAP5 was added to the imaging chamber at *t0*. Blue lines indicate the mean; red lines indicate the SEM. The inositol 1,4,5-triphosphate receptor inhibitor xestospongin C abrogated calcium mobilization, while inhibition of ryanodine receptor with ryanodine did not prevent calcium mobilization. (**F**) Mean normalized time courses of store-operated calcium entry. Thapsigargin was used to empty intracellular Ca^{2+} stores in the absence of extracellular Ca^{2+}. Addition of Ca^{2+} to the medium at *t0* resulted in rapid extracellular Ca^{2+} entry, which was inhibited by preincubation with SKF96365. Solid lines indicate the mean. Dotted lines indicate the SEM. (**G**) Western blot analyses showing that hMEC-1 and TIME endothelial cells treated with recMFAP5 had higher expression of p-FAK (Y861), p–PLC-γ1 (Y783), p-PKCθ (T538), p-ERK1/2 (T202/Y204), p-MLC2 (T18/S19), p-CREB (S133), c-Jun, and p–c-Jun (S73) compared with control cells. Relative normalized protein expression levels with respect to the corresponding controls are shown. Note: The blot groupings for p-CREB in hMEC-1 and TIME MECs and p-PKCθ in TIME MECs were generated from multiple gels that were run in parallel. (**H**) MFAP5-induced microvascular endothelial cell motility was suppressed in MECs treated with anti–$\alpha_v\beta_3$ integrin antibodies. hMEC-1 and TIME MECs were treated with 50 ng/ml recMFAP5 in the presence of an anti-α_5 antibody, an anti-$\alpha_v\beta_3$ antibody, or the control IgG, and the effect on cell motility was determined by a Boyden chamber cell motility assay (mean ± SEM of 3 independent experiments; $P < 0.01$, by 2-tailed Student's *t* test).

injected twice weekly via the tail vein with chitosan nanoparticles incorporated with 1 of 2 different murine *Mfap5*–targeting siRNAs or control scrambled siRNA for a total of 6 weeks. Tumor progression was monitored using an IVIS 200 Bioluminescence and Fluorescence Imaging System (Caliper Life Sciences) throughout the course of the experiment. By week 6, all animals were euthanized, and tumor tissues were resected and weighted. Immunolocalization of murine Mfap5, CD34, and Lpp on paraffin-embedded sections of ovarian tumors from mice was performed.

In vivo implantation of Matrigel plugs. To determine the extent to which MFAP5 protein promotes endothelial *LPP* expression, tumor progression, and angiogenesis in vivo, mice were implanted i.p. with Matrigel plugs reconstituted in recMFAP5 or control buffer. Five days after implantation, the Matrigel plugs were resected, and a phenotypic analysis of CD31-positive endothelial cells was performed using the angiogenesis module of MetaMorph Imaging Analysis software (Molecular Devices). To determine whether recMfap5 directly upregulates endothelial *Lpp* in vivo, we performed transcriptome profiling on total RNA samples isolated from mouse endothelial cells that invaded into the Matrigel plugs. Total RNA (100 ng) from each group of Matrigel plugs was used to generate biotin-labeled RNA with a MessageAmp Premier RNA Amplification Kit (Life Technologies, Thermo Fisher Scientific) according to the manufacturer's protocol. Biotin-labeled RNA samples from mouse endothelial cells were then subjected to whole-genome transcriptome profiling using a GeneChip Mouse Genome 430 2.0 Array (Affymetrix). qRT-PCR and immunostaining were performed to further validate the upregulation of *LPP* expression by MFAP5.

Accession numbers. Data files from the transcriptome profiling analysis were deposited in the NCBI's Gene Expression Omnibus (GEO) database (GEO GSE70344 and GSE106519).

Statistics. SPSS 19 (IBM Corporation) and GraphPad Prism 5.0 (GraphPad Software) were used to perform statistical analyses. All in vitro experiments were repeated independently in triplicate, and a 2-tailed Student's *t* test was used to determine differences in sample means. The Mann-Whitney *U* test was used in animal studies. For transcriptome analyses, Genespring GX Bioinformatics Suite, version 14.9 (Agilent Technologies) was used. A *P* value of less than 0.05 was considered statistically significant, and a moderated *t* test and Benjamini-Hochberg multiple testing correction were used as appropriate.

Study approval. Patients' tissue samples were collected from the Ovarian Cancer Repository under protocols approved by the IRB of The University of Texas MD Anderson Cancer Center, and all animal experiments were approved by the IACUC of The University of Texas MD Anderson Cancer Center.

Additional information is provided in the Supplemental Methods.

Author contributions

CSL, TLY, MJB, and SCM conceptualized the study. CSL, TLY, KPY, SYH, LSM, AKS, and GLB designed the experiments. CSL, TLY, KKW, JS, and STCW performed formal data analysis. CSL, TLY, KPY, and SYH conducted the experiments. CSL, TLY, KPY, JS, STCW, MJB, and SCM wrote the manuscript. MJB and SCM supervised the study.

Acknowledgments

This study was supported in part by NIH grants (R01 CA133057, R01 CA142832, RC4 CA156551, U54 CA151668, U01 188388, CA177909, and UH2 TR000943); a University of Texas MD Anderson Cancer Center Ovarian Cancer Specialized Programs of Research Excellence (SPORE) grant (P50 CA083639), a Uterine Cancer SPORE grant (P50 CA098258), and an NIH Cancer Center Support grant (P30 CA016672); the U.S. Department of Health and Human Services; the Gilder Foundation; Cancer Prevention & Research Institute of Texas grants (RP100094 and RP110595); US Department of Defense grants (W81XWH-16-2-0038 and W81XWH-17-1-0126); the Mary K. Chapman Foundation; and the Ovarian Cancer Research Fund. Editorial support was provided by the Department of Scientific Publications at The University of Texas MD Anderson Cancer Center.

Address correspondence to: Samuel C. Mok, Department of Gynecologic Oncology and Reproductive Medicine, Unit 1362, The University of Texas MD Anderson Cancer Center, 1515 Holcombe Boulevard, Houston, Texas 77030, USA. Phone: 713.792.1442; Email: scmok@mdanderson.org. Or to: Michael J. Birrer, Comprehensive Cancer Center, Division of Hematology-Oncology, University of Alabama at Birmingham, Birmingham, 1824 Sixth Avenue, WTI 202, Birmingham, Alabama 35294, USA. Phone: 205.934.5077; Email: mbirrer@uab.edu.

1. Choi HJ, Armaiz Pena GN, Pradeep S, Cho MS, Coleman RL, Sood AK. Anti-vascular therapies in ovarian cancer: moving beyond anti-VEGF approaches. *Cancer Metastasis Rev*. 2015;34(1):19–40.
2. Burger RA. Overview of anti-angiogenic agents in development for ovarian cancer. *Gynecol Oncol*. 2011;121(1):230–238.
3. Perren TJ, et al. A phase 3 trial of bevacizumab in ovarian cancer. *N Engl J Med*. 2011;365(26):2484–2496.
4. Aghajanian C, et al. OCEANS: a randomized, double-blind, placebo-controlled phase III trial of chemotherapy with or without bevacizumab in patients with platinum-sensitive recurrent epithelial ovarian, primary peritoneal, or fallopian tube cancer. *J Clin Oncol*. 2012;30(17):2039–2045.
5. Pujade-Lauraine E, et al. Bevacizumab combined with chemotherapy for platinum-resistant recurrent ovarian cancer: The AURELIA open-label randomized phase III trial. *J Clin Oncol*. 2014;32(13):1302–1308.
6. Orimo A, Weinberg RA. Stromal fibroblasts in cancer: a novel tumor-promoting cell type. *Cell Cycle*. 2006;5(15):1597–1601.
7. Yeung TL, Leung CS, Li F, Wong SS, Mok SC. Targeting stromal-cancer cell crosstalk networks in ovarian cancer treatment. *Biomolecules*. 2016;6(1):3.
8. Yeung TL, et al. TGF-β modulates ovarian cancer invasion by upregulating CAF-derived versican in the tumor microenvironment. *Cancer Res*. 2013;73(16):5016–5028.
9. Mueller MM, Fusenig NE. Friends or foes - bipolar effects of the tumour stroma in cancer. *Nat Rev Cancer*. 2004;4(11):839–849.
10. Kitadai Y. Cancer-stromal cell interaction and tumor angiogenesis in gastric cancer. *Cancer Microenviron*. 2010;3(1):109–116.
11. Au Yeung CL, et al. Exosomal transfer of stroma-derived miR21 confers paclitaxel resistance in ovarian cancer cells through targeting APAF1. *Nat Commun*. 2016;7:11150.
12. Petit MM, Mols R, Schoenmakers EF, Mandahl N, Van de Ven WJ. LPP, the preferred fusion partner gene of HMGIC in lipomas, is a novel member of the LIM protein gene family. *Genomics*. 1996;36(1):118–129.
13. Petit MM, et al. LPP, an actin cytoskeleton protein related to zyxin, harbors a nuclear export signal and transcriptional activation capacity. *Mol Biol Cell*. 2000;11(1):117–129.
14. Van Itallie CM, et al. Biotin ligase tagging identifies proteins proximal to E-cadherin, including lipoma preferred partner, a regulator of epithelial cell-cell and cell-substrate adhesion. *J Cell Sci*. 2014;127(Pt 4):885–895.
15. Zhang H, Chen X, Bollag WB, Bollag RJ, Sheehan DJ, Chew CS. Lasp1 gene disruption is linked to enhanced cell migration and tumor formation. *Physiol Genomics*. 2009;38(3):372–385.
16. Thibault B, Castells M, Delord JP, Couderc B. Ovarian cancer microenvironment: implications for cancer dissemination and chemoresistance acquisition. *Cancer Metastasis Rev*. 2014;33(1):17–39.
17. Jain RK. Normalization of tumor vasculature: an emerging concept in antiangiogenic therapy. *Science*. 2005;307(5706):58–62.
18. Leung CS, et al. Calcium-dependent FAK/CREB/TNNC1 signalling mediates the effect of stromal MFAP5 on ovarian cancer metastatic potential. *Nat Commun*. 2014;5:5092.
19. Ingber DE, Folkman J. Mechanochemical switching between growth and differentiation during fibroblast growth factor-stimulated angiogenesis in vitro: role of extracellular matrix. *J Cell Biol*. 1989;109(1):317–330.
20. Matsumoto T, Yung YC, Fischbach C, Kong HJ, Nakaoka R, Mooney DJ. Mechanical strain regulates endothelial cell patterning in vitro. *Tissue Eng*. 2007;13(1):207–217.
21. Ghosh K, Thodeti CK, Dudley AC, Mammoto A, Klagsbrun M, Ingber DE. Tumor-derived endothelial cells exhibit aberrant Rho-mediated mechanosensing and abnormal angiogenesis in vitro. *Proc Natl Acad Sci U S A*. 2008;105(32):11305–11310.
22. Scherr DS. Commentary on "tissue-specific mutagenesis by N-butyl-N-(4-hydroxybutyl) nitrosamine as the basis for urothelial cell carcinogenesis." He Z, Kosinska W, Zhao ZL, Wu XR, Guttenplan JB, Department of Basic Science, New York University Dental College, NY, USA.: Mutat Res 2012;742(1-2):92-5 [Epub 2011 Dec 4]. *Urol Oncol*. 2014;32(2):214.
23. Califano JP, Reinhart-King CA. Exogenous and endogenous force regulation of endothelial cell behavior. *J Biomech*. 2010;43(1):79–86.
24. Krishnan R, et al. Substrate stiffening promotes endothelial monolayer disruption through enhanced physical forces. *Am J Physiol, Cell Physiol*. 2011;300(1):C146–C154.
25. Kerr JS, Mousa SA, Slee AM. Alpha(v)beta(3) integrin in angiogenesis and restenosis. *Drug News Perspect*. 2001;14(3):143–150.
26. Eddy RJ, Pierini LM, Matsumura F, Maxfield FR. Ca2+-dependent myosin II activation is required for uropod retraction during neutrophil migration. *J Cell Sci*. 2000;113(Pt 7):1287–1298.
27. Lawson MA, Maxfield FR. Ca(2+)- and calcineurin-dependent recycling of an integrin to the front of migrating neutrophils. *Nature*. 1995;377(6544):75–79.
28. Coppolino MG, Woodside MJ, Demaurex N, Grinstein S, St-Arnaud R, Dedhar S. Calreticulin is essential for integrin-mediated calcium signalling and cell adhesion. *Nature*. 1997;386(6627):843–847.
29. Manicassamy S, Sadim M, Ye RD, Sun Z. Differential roles of PKC-theta in the regulation of intracellular calcium concentration in primary T cells. *J Mol Biol*. 2006;355(3):347–359.
30. Nakamura I, Lipfert L, Rodan GA, Le TD. Convergence of alpha(v)beta(3) integrin- and macrophage colony stimulating factor-mediated signals on phospholipase Cgamma in prefusion osteoclasts. *J Cell Biol*. 2001;152(2):361–373.
31. Masson-Gadais B, Houle F, Laferrière J, Huot J. Integrin alphavbeta3, requirement for VEGFR2-mediated activation of SAPK2/p38 and for Hsp90-dependent phosphorylation of focal adhesion kinase in endothelial cells activated by VEGF. *Cell Stress Chaperones*. 2003;8(1):37–52.
32. Curtis J, Finkbeiner S. Sending signals from the synapse to the nucleus: possible roles for CaMK, Ras/ERK, and SAPK pathways in the regulation of synaptic plasticity and neuronal growth. *J Neurosci Res*. 1999;58(1):88–95.
33. Mavria G, et al. ERK-MAPK signaling opposes Rho-kinase to promote endothelial cell survival and sprouting during angiogenesis. *Cancer Cell*. 2006;9(1):33–44.
34. Hansen MD, Beckerle MC. Alpha-Actinin links LPP, but not zyxin, to cadherin-based junctions. *Biochem Biophys Res Commun*. 2008;371(1):144–148.
35. Hashizume H, et al. Openings between defective endothelial cells explain tumor vessel leakiness. *Am J Pathol*. 2000;156(4):1363–1380.
36. McDonald DM, Baluk P. Significance of blood vessel leakiness in cancer. *Cancer Res*. 2002;62(18):5381–5385.
37. Trédan O, Galmarini CM, Patel K, Tannock IF. Drug resistance and the solid tumor microenvironment. *J Natl Cancer Inst*. 2007;99(19):1441–1454.
38. Goel S, Wong AH, Jain RK. Vascular normalization as a therapeutic strategy for malignant and nonmalignant disease. *Cold Spring Harb Perspect Med*. 2012;2(3):a006486.
39. Goel S, et al. Normalization of the vasculature for treatment of cancer and other diseases. *Physiol Rev*. 2011;91(3):1071–1121.
40. Jain RK. Taming vessels to treat cancer. *Sci Am*. 2008;298(1):56–63.
41. Padera TP, Stoll BR, Tooredman JB, Capen D, di Tomaso E, Jain RK. Pathology: cancer cells compress intratumour vessels. *Nature*. 2004;427(6976):695.
42. Bergers G, Hanahan D. Modes of resistance to anti-angiogenic therapy. *Nat Rev Cancer*. 2008;8(8):592–603.
43. Yeung TL, Leung CS, Yip KP, Au Yeung CL, Wong ST, Mok SC. Cellular and molecular processes in ovarian cancer metastasis. A Review in the Theme: Cell and Molecular Processes in Cancer Metastasis. *Am J Physiol, Cell Physiol*. 2015;309(7):C444–C456.